AD-761 200

CERAMIC MATERIALS IN ROLLING CONTACT BEARINGS

NORTON COMPANY

PREPARED FOR

NAVAL AIR SYSTEMS COMMAND

FEBRUARY 1973

Distributed By:

NTIS

National Technical Information Service
U. S. DEPARTMENT OF COMMERCE

AD 761200

CERAMIC MATERIALS IN ROLLING CONTACT BEARINGS

FINAL REPORT
Contract N00019-72-C-0299
January 3, 1972 to February 3, 1973

W. M. Wheildon
H. R. Baumgartner
D. V. Sundberg
M. L. Torti

SUBMITTED TO:

Department of the Navy
Naval Air Systems Command
Code AIR-52032A
Washington D. C. 20360

Reproduced by
NATIONAL TECHNICAL
INFORMATION SERVICE
U S Department of Commerce
Springfield VA 22151

DDC
JUN 8 1973
B

Approved for public release; distribution unlimited.

NORTON COMPANY
INDUSTRIAL CERAMICS DIVISION
WORCESTER, MASSACHUSETTS 01606

UNCLASSIFIED
Security Classification

DOCUMENT CONTROL DATA - R & D

(Security classification of title, body of abstract and indexing annotation must be entered when the overall report is classified)

1. ORIGINATING ACTIVITY (Corporate author)

Norton Company, Industrial Ceramics Division
1 New Bond Street
Worcester, Massachusetts 01606

2a. REPORT SECURITY CLASSIFICATION

2b. GROUP

3. REPORT TITLE

CERAMIC MATERIALS IN ROLLING CONTACT BEARINGS

4. DESCRIPTIVE NOTES (Type of report and inclusive dates)

Final (January 3, 1972 to February 3, 1973)

5. AUTHOR(S) (First name, middle initial, last name)

William M. Wheildon
H Robert Baumgartner
David V. Sundberg
Maurice L. Torti

6. REPORT DATE

February 1973

7a. TOTAL NO. OF PAGES

97

7b. NO. OF REFS

13 Tables
53 Figures

8a. CONTRACT OR GRANT NO.

N00019-72-C-0299

b. PROJECT NO

c.

d.

9a. ORIGINATOR'S REPORT NUMBER(S)

9b. OTHER REPORT NO(S) (Any other numbers that may be assigned this report)

10. DISTRIBUTION STATEMENT

APPROVED FOR PUBLIC RELEASE; DISTRIBUTION UNLIMITED

11. SUPPLEMENTARY NOTES

12. SPONSORING MILITARY ACTIVITY

Department of the Navy
Naval Air Systems Command
Washington, D.C. 20360

13. ABSTRACT

The Naval Air Systems Command Contract N00019-72-C-0299 for investigation of ceramic materials in rolling contact bearings, was carried out with high strength silicon nitride, silicon carbide and aluminum oxide.

Screening rolling contact fatigue testing on silicon nitride with conventional lubricants showed excellent life, greater than M50 steel, at comparable load.

The friction and wear properties were determined for silicon nitride, silicon carbide and steel. The coefficient of friction and wear rates are nearly the same for steel-steel and steel-silicon nitride combinations.

The corrosion resistance of silicon nitride is excellent in hot Type II turbo oil.

The dimensional stabilities of silicon nitride and silicon carbide are excellent and do not present a problem in designing bearing clearances.

Full scale test bearing rollers made from silicon nitride fractured during final shaping by grinding and new grinding techniques are being developed for additional roller manufacture.

An extensive investigation into surface damage by grinding indicates surface preparation techniques are important.

DD FORM 1 NOV 65 1473 REPLACES DD FORM 1473, 1 JAN 64, WHICH IS OBSOLETE FOR ARMY USE.

UNCLASSIFIED
Security Classification

14. KEY WORDS	LINK A ROLE	LINK A WT	LINK B ROLE	LINK B WT	LINK C ROLE	LINK C WT
Ceramic						
Silicon nitride (Si_3N_4)						
Silicon carbide (SiC)						
Aluminum oxide (Al_2O_3)						
High Strength						
Rolling Contact Fatigue (RCF)						
Friction						
Wear						
Corrosion resistance						
Stability						
Surface preparation						
Bearing rollers						

ia

CERAMIC MATERIALS IN ROLLING CONTACT BEARINGS

FINAL REPORT

CONTRACT N00019-72-C-0259
January 3, 1972 to February 3, 1973

W. M. Wheildon
H. R. Baumgartner
D. V. Sundberg
M. L. Torti

SUBMITTED TO:

Department of the Navy
Naval Air Systems Command
Code AIR-52032A
Washington D. C. 20360

Approved for public release; distribution unlimited.

NORTON COMPANY
INDUSTRIAL CERAMICS DIVISION
WORCESTER, MASSACHUSETTS 01606

16

TABLE OF CONTENTS

	PAGE
Foreword	
Abstract	
Summary	
I. Introduction	1
II. Materials Selection and Characterization	2
III. Screening Tests	2
A. RCF (Rolling Contact Fatigue)	2
1. Description of Equipment	
2. Material Preparation	
3. Results	
B. Four-Ball Testing	12
1. Description of Equipment	
2. Material Preparation	
3. Results	
C. Friction and Wear Testing	20
D. Environmental Testing	24
1. Dimensional Stability	
2. Effects on Fatigue Life	
3. Lubricant Shut-Off and Entrained Particles	
IV. Full Scale Bearing	28
A. Design	28
B. Test Equipment and Procedures	32
C. Materials Fabrication	32
1. Metal Components	
2. Ceramic Bearing Roller Preparation	
D. Analysis of Rolling Contact Fatigue Test Results	40
1. Introduction	
2. Experimental Observations	
3. Discussion	
4. Summary and Conclusions	
E. Replacement Bearing Rollers	72
V. Conclusions and Recommendations	73
A. Conclusions	73
B. Recommendations	73
Appendix I Ceramics in Rolling Contact Bearings Prior Work	74
Appendix II Hertz Stress Calculations	76
Bibliography	77

LIST OF TABLES

TABLE NUMBER		PAGE
I	Typical Physical Properties of Candidate Ceramic Materials	3
II	Typical Metallic Constituents of Candidate Ceramic Materials	4
III	Rolling Contact Fatigue Life - Hot Pressed Silicon Nitride	8
IV	Chemical Analysis and Hardness of RCF Rods	10
V	Rolling Contact Fatigue Life - Hot Pressed SiC and Dense Sintered Al_2O_3	15
VI	Four-Ball Test Results	21
VII	Wear Test Results at 50 Pounds Load and 75°F	25
VIII	Dimensional Stability of Silicon Nitride and Silicon Carbide Compared to M-50 CVM	26
IX	Rolling Contact Fatigue Life HS-110A Silicon Nitride Environmental Exposure Tests	29
X	Effect of Silicon Carbide Grinding on Fatigue Life of HS-110A Si_3N_4	35
XI	Dimensional Characteristics of Twenty Si_3N_4 Roller Blanks	36
XII	Rolling Contact Fatigue Life of HS-110A Si_3N_4 Bearing Roller Billets	38
XIII	Summary of Selected Information on the RCF Rods	41

LIST OF FIGURES

FIGURE NUMBER		PAGE
1	Rolling Contact Fatigue Test Machines	5
2	Weibull Slope of Silicon Nitride	11
3	Silicon Nitride and M-50 RCF Rod Fatigue Spalls	13
4.	Spall in Silicon Nitride RCF Rod	14
5	Linear Proficording Across Test Track on AD999 Aluminum Oxide Bar #1	16
6	Linear Proficording Across Test Tracks on M-50 CVM	17
7	Federal-Mogul Four Ball Test Machine	18
8	Schematic of the Four-Ball Tester	19
9	Surface of Silicon Nitride Ball	22
10	Hohman A-6 Wear Test Machine	23
11	Dimensional Stability Measurement Set-Up	27
12	Bearing Roller Design	30
13	Ceramic Bearing Assembly	31
14	Variable Speed Bearing Test Machine	33
15	Bearing Test Adapters and Support Bearings	34
16	Surface as finished with a 320 grit diamond wheel. Rod FM-1	42
17	Surface as finished with impregnated leather lap on the 320 grit ground surface. Rod FM-3	43
18	Surface as finished with impregnated leather lap showing residual grinding scratches Rod FM-4	43
19	Surface as reground lightly with a silicon carbide wheel. Rod FM-7	44
20	Surface as finished by machine lapping after grinding with a 100 grit wheel. Rod #12	44

LIST OF FIGURES
(continued)

FIGURE NUMBER		PAGE
21	Surface as finished by machine lapping showing random lapping scratches. Rod #15	45
22	Relatively large and deep surface pits on, and unique to. Rod #12	45
23	Wear spall on Rod FM-1	46
24	Wear spall on Rod FM-3	47
25	Wear spall on Rod FM-11	47
26	Wear spall on Rod #8	49
27	Wear spall on Rod #12	49
28	Wear spall on Rod #13	50
29	Higher magnification of RHS portion of spall in Figure 25	50
30	Enlargement of pit above center in Figure 27	51
31	Possible exposed pore or surface pit on wall of spall. Rod #15	51
32	Appearance after fatigue testing of 320 grit ground surface	53
33	Appearance after fatigue testing of leather lapped surface. Rod FM-3	53
34	Appearance after fatigue testing of surface reground with SiC wheel. Rod FM-7	54
35	Appearance after fatigue testing of surface machine lapped after 100 grit grind. Rod #12	54
36	Higher magnification of worn 320 grit ground surface showing elongated pits and stepped appearance. Rod FM-1	55
37	Higher magnification of surface finished with 320 grit wheel. Rod FM-1	55
38	Another example of worn track on a leather lapped surface. Rod FM-4	56

LIST OF FIGURES
(continued)

FIGURE NUMBER		PAGE
39	Example of development of large pits in loaded track. Rod #13	57
40	Example of development of large pits in loaded track. Rod #15	57
41	Porosity in Rod #12 Phase-interference contrast microscopy	59
42	Porosity in Rod #8 Phase-interference contrast microscopy	59
43	Porosity in Rod FM-7 Phase-interference contrast microscopy	60
44	Porosity in Rod FM-10 Phase-interference microscopy	60
45A	Polished surface of Rod #12. Plane-polarized light	61
45B	Same area as in Figure 45A Cross-polarized light	61
46A	Polished surface of Rod #8. Plane-polarized light	62
46B	Same area as in Figure 46A. Cross-polarized light	62
47A	Polished surface of Rod FM-7 Plane-polarized light	63
47B	Same area as in Figure 47A. Cross polarized light	63
48A	Polished surface of Rod FM-10. Plane-polarized light	64
48B	Same area as in Figure 48A. Cross-polarized light	64
49A	Porosity in Rod #12	65
49B	Higher magnification of pit towards lower left corner in Figure 49A	65

LIST OF FIGURES
(continued)

FIGURE NUMBER		PAGE
50	Porosity in Rod #8	66
51	Porosity in Rod FM-7	66
52	Porosity in Rod FM-10	67
53	Grinding scratch with associated pitting damage on polished silicon nitride	70

FOREWORD

This report covers activities carried out by Norton Company, Worcester, Massachusetts, 01606, under Naval Air Systems Command Contract N00019-72-C-0299, initiated to "investigate the utility of ceramic materials in rolling contact bearings". The work was administered under the direction of Mr. Charles F. Bersch, NAVAIR, Washington, D.C.

The following Norton personnel were major contributors to the program in the capacity noted:

W. M. Wheildon - - - Principal Investigator
H. R. Baumgartner - - Failure Analyses
M. L. Torti - - - Technical Management

Bearing design and testing facilities were supplied by Federal Mogul Corporation, Ann Arbor, Michigan, 48104, under subcontract to Norton Company,

D. V. Sundberg - - - Principal Investigator

ABSTRACT

The Naval Air Systems Command Contract N00019-72-C-0299 for investigation of ceramic materials in rolling contact bearing was carried out primarily with high strength silicon nitride and to a lesser degree assessments were made of silicon carbide and aluminum oxide.

Screening rolling contact fatigue testing on silicon nitride with conventional lubricants showed excellent life, greater than M50 steel, at comparable loads. Rolling contact fatigue tests of silicon carbide and aluminum oxide did not show as much promise as silicon nitride.

The friction and wear properties were determined for silicon nitride, silicon carbide and steel. The coefficient of friction and wear rates are nearly the same for steel-steel and steel-silicon nitride combinations. Based on these results, excessive wear is not expected in a full scale bearing with silicon nitride rollers.

The corrosion resistance of silicon nitride is excellent in hot Type II Turbo oil.

The dimensional stabilities of silicon nitride and silicon carbide are excellent and do not present a problem in designing bearing clearances.

Full scale test bearing rollers made from silicon nitride fractured during final shaping by grinding and new grinding techniques are being developed for additional roller manufacture.

Rolling contact fatigue tests carried out on the billets from which the roller blanks were taken failed to duplicate the original results. An extensive investigation of this discrepancy led to the conclusion that subsurface damage caused by a change in surface preparation techniques was responsible.

Billets of a newer still higher purity silicon nitride have been pressed as stock for additional roller manufacture. Rods cut from these billets with surfaces prepared by the original diamond grinding techniques have given initial rolling contact fatigue life results that support the original testing.

SUMMARY

This investigation can be divided into two principal activities; (1) ceramic bearing material selection, screening and characterization relying principally upon rolling contact fatigue testing of rod specimens and (2) high speed roller bearing design (ceramic rollers with metal races), component fabrication, and analyses.

The materials selected for screening were hot pressed silicon nitride and silicon carbide and dense high purity alumina, based primarily on high strength, low porosity and high hardness considerations. The silicon nitride and silicon carbide test rods were cut from billets hot pressed by Norton Company. The aluminum oxide was supplied to the final test configuration by Coors Porcelain Company.

The Rolling Contact Fatigue (RCF) test machine is a rapid method of evaluating bearing materials under load. A small rod specimen is loaded between two relatively large diameter opposing crowned wheels that apply pressure while the specimen is driven at 10,000 rpm. The specimen receives two stress cycles per revolution resulting in 1.2×10^6 test cycles per hour. All testing was carried out with conventional lubrication.

A condensed table of the most significant rolling contact fatigue screening test results is given below:

Rolling Contact Fatigue
800,000 psi calculated Hertz stress

Material	No. of tests	Cycles to Failure	
		10 percentile (L_{10})	median
Silicon nitride HS110A	26	5,690,000	30,650,000
Silicon nitride HS130	5	-	5,119,000
Silicon carbide HX294	1	-	<1,000
Aluminum oxide Coors AD999	Testing limited to 700,000 psi maximum Hertz stress		
M-50 *CVM	34	1,820,000	3,660,000

*Bearing steel control - carried out at the same load as the silicon nitride resulting in a calculated Hertz stress of 700,000 psi.

Hot pressed silicon nitride (HS110A process) performed significantly better than the M-50 bearing steel control material. In addition silicon nitride failures were characterized by the appearance of a small spall very similar to that encountered with the

bearing steel. Limited testing of HS130 produced results comparable to those obtained on the bearing steel.

Hot pressed silicon carbide did not generally fail by spalling but had a tendency to massive brittle fracture and attempts to operate at 800,000 psi Hertz calculated stress resulted in rod breakage at less than 1000 cycles. A reduction to 700,000 psi Hertz stress allowed operation up to 17,500,000 cycles although the rod did fracture upon removal. A further reduction in stress to 600,000 psi extended life to 24,000,000 cycles.

Aluminum oxide was tested at calculated Hertz stresses from 500,000 to 700,000 psi but cannot be compared to other roller materials as it wears continuously and excessively by crushing under all loads applied and has no typical spalling end point.

Consequently HS110A silicon nitride was selected as the prime candidate for further environmental testing and for roller fabrication for testing in an actual roller bearing (with M-50 steel races). However, some further environmental testing was also carried out on hot-pressed silicon carbide.

A limited amount of four ball testing was carried out on HS110B silicon nitride with generally poor results compared to M-50 steel. Since, in this case, both ball dimensional and starting material quality was suspect it is not felt that these results were definitive.

Friction and wear properties were determined for silicon nitride, silicon carbide and steel combinations. The coefficient of friction and wear removal rates are nearly the same as for steel-steel and steel-silicon nitride combinations. Based on these results, excessive wear should not be encountered in a bearing containing silicon nitride rollers.

The corrosion resistance of silicon nitride is excellent in hot Type II turbo oil. Fatigue results before and after exposure are inconclusive because of the short duration of the initial tests. The dimensional stability of silicon nitride and silicon carbide is excellent and does not present a problem in designing bearing clearances.

A test roller bearing was designed based upon a high speed aircraft quality steel bearing. The test bearing has twenty ceramic rollers 0.345 inch diameter and length. The M-50 steel races have a 2.25 inch bore and 3.740 inch outer diameter.

Plates, 6" x 6" x 5/8" of HS110A hot pressed silicon nitride were sectioned and 130 roller blanks 0.356 x 0.356 inch were diamond ground.

It was planned to apply the final dimensional accuracies and contour to these by standard bearing grinding procedures using

silicon carbide wheels. An inadvertent error in wheel selection in the bearing plant damaged or destroyed these rollers.

Rolling contact fatigue (RCF) test rods cut from the same billets the rollers were taken were tested yielding lives an order of magnitude poorer than the screening test results. This shorter life triggered an extensive investigation into both the surface finish and material qualities of the two groups of material. It was concluded that the premature failure of the second group was linked to rapid surface pit formation during RCF testing leading to a spalling type failure. It is felt that this rapid pit formation was caused by surface damage not removed in the final rod preparation. The grinding practice for the first set of rods contained a finish grind with a 320 grit diamond wheel followed by 6μ diamond hand lapping. In the second group this 320 grit finish grinding step was omitted prior to a final mechanical lapping with 6μ diamond.

Preliminary test results (to be reported in the next period) on RCF rods of the replacement material with surfaces prepared in the original manner are more in line with the initial results.

I. INTRODUCTION

Ceramic materials offer many interesting properties which suggest their use in bearings. Among these are; light weight, high mechanical strength in compression, resistance to corrosion, low coefficient of friction, dimensional stability, and high hardness over a wide temperature range. In addition they are generally further characterized by high resistance to wear, low coefficient of thermal expansion, very high melting point, and the ability to hold close tolerances and fine finishes. Because of the desirability of many of these properties, extensive studies have been conducted with both solid ceramic and ceramic coatings for sliding and plain bearings. This work has lead to wide use of ceramic containing plain bearings in industry.

Though numerous studies have been conducted and others are continuing with ceramics for plain and gas bearings, limited work has been devoted to ceramics for rolling contact (ball and/or roller) bearings. More importantly, even less work has been done with what might be termed advanced ceramics. Advanced ceramics would include those materials having very high cross-bending strengths, very fine grain size, high density, and a very homogeneous structure. For background, Appendix I summarizes much of the work to date with ceramics in rolling contact.

These properties plus stable characteristics at elevated temperatures has identified advanced ceramics as excellent potential candidate materials for applications involving rolling contact environments at elevated temperatures such as aircraft engine roller bearings.

High rotational speeds developed in modern jet engines have changed the common failure mode of both roller and ball bearings to the outer race instead of the inner race. The high centrifugal forces of the rollers developed by the increased speeds have loaded the outer races to the point where they must endure higher stresses than the inner races. Hollow steel balls have been investigated but fabrication problems influencing balance limits their usefulness at high speeds. Light weight ceramics with specific gravities two-fifths that of steel would greatly reduce centrifugal loading even when used in the solid form.

The present program was undertaken to investigate high strength ceramics as rolling contact bearing for aircraft engine applications. The program is broadly divided into two phases: (1) materials investigation and evaluation and (2) full bearing fabrication and testing.

II. MATERIALS SELECTION AND CHARACTERIZATION

Four materials were selected for screening evaluation based primarily on their strength, density and hardness characteristics. These are two forms of hot-pressed silicon nitride, hot-pressed silicon carbide and a dense sintered aluminum oxide. Typical properties and chemical analyses are given in Tables I and II.

The hot-pressed silicon nitride and silicon carbide were supplied to the program in the form of hot pressed plates prepared from Norton synthesized starting materials.

The aluminum oxide rods were purchased from the Coors Porcelain Company in the finished form.

III. SCREENING TESTS

A. RCF (Rolling Contact Fatigue)

1. Description of Equipment - The Rolling Contact Fatigue (RCF) test machine developed by General Electric Company and marketed by Polymet Corporation was the primary means of evaluating material fatigue life throughout the program, Figure 1. Two discs, seven inches in diameter and one-half inch thick, are held against the rotating test specimen. The discs have a crown radius of 0.250 inches. The test specimen is a straight cylinder three inches long with a diameter of 0.375 inches. With this geometry configuration, the contact stresses can be calculated (in the non-lubricated condition) as shown in Appendix II. The example of this calculation in the appendix shows for a load of 325 pounds, the maximum Hertz compressive stress is 700,000 psi for steel wheels and a steel test specimen. The load necessary to produce this stress in the ceramic materials tested is less than 325 pounds because of their higher moduli of elasticity.

The RCF machine provides a means of rapid testing in pure rolling contact. Since the specimen receives two stress cycles for each revolution, 10,000 rpm of the specimen gives 1.2×10^6 cycles per hour. The average M-50 test is about 3.5×10^6 cycles so an average test lasts three hours. In contrast, the average "accelerated" full scale bearing test has a duration of about 500 hours.

The loading discs see a comparable stress to the test specimen, but their relatively large diameter provides a longer life than the specimens. However, they require refinishing when they spall or flatten, usually after 20-30 tests on steel. The discs are requalified after grinding using a controlled group of M-50 steel specimens.

The test conditions on the RCF machines used throughout this program were:

TABLE I

Typical Physical Properties

	Si_3N_4 HS110A&B	Si_3N_4 HS-130	SiC HX-294	Al_2O_3[1] AD999
Flexural Strength psi 1/8x1/8 rods 3 point bend @ 75°F	120,000	130,000	110,000	105,000[2]
@ 2500°F	25,000	50,000	70,000	-
Compressive Strength psi @ 75°F	500,000	500,000	500,000	650,000
Modulus of Elasticity psi (Sonic) @ 75°F	45×10^6	46×10^6	64×10^6	56×10^6
Coefficient of Linear Thermal Expansion 75 - 300°F /°F	1.8×10^{-6}	1.8×10^{-6}	2.7×10^{-6}	3.8×10^{-6}
Thermal Conductivity BTU/hr ft°F @ 75°F		18	47	18
Specific Heat @ 75°F	0.17	0.17	0.15	0.21
Electrical Resistivity ohm-cm @ 75°F	10^{11}	10^{11}	10^{-1}-10^{3}	$>10^{15}$
Hardness Knoop K_{100}	2200	2200	2500	-
R_{45N}	-	-	-	90
Density gm/cc	3.15	3.18	3.30	3.90

(1) Coors Porcelain Company, Bulletin No. 953.
(2) Tested per ASTM C-369-66T

TABLE II

Typical Metallic Constituents Analysis
weight percent

	Si_3N_4			SiC	Al_2O_3
	HS-110A	HS-110B	HS-130	HX-294	AD999
Aluminum	0.6	0.6	0.2	2	Nominal
Iron	0.5	0.5	0.3	0.1	99.9% Al_2O_3
Ca	0.25	0.25	0.08	<0.05	
Mg	0.6	0.6	0.6	<0.05	
W	<0.01	1.4	1.4	2.5	

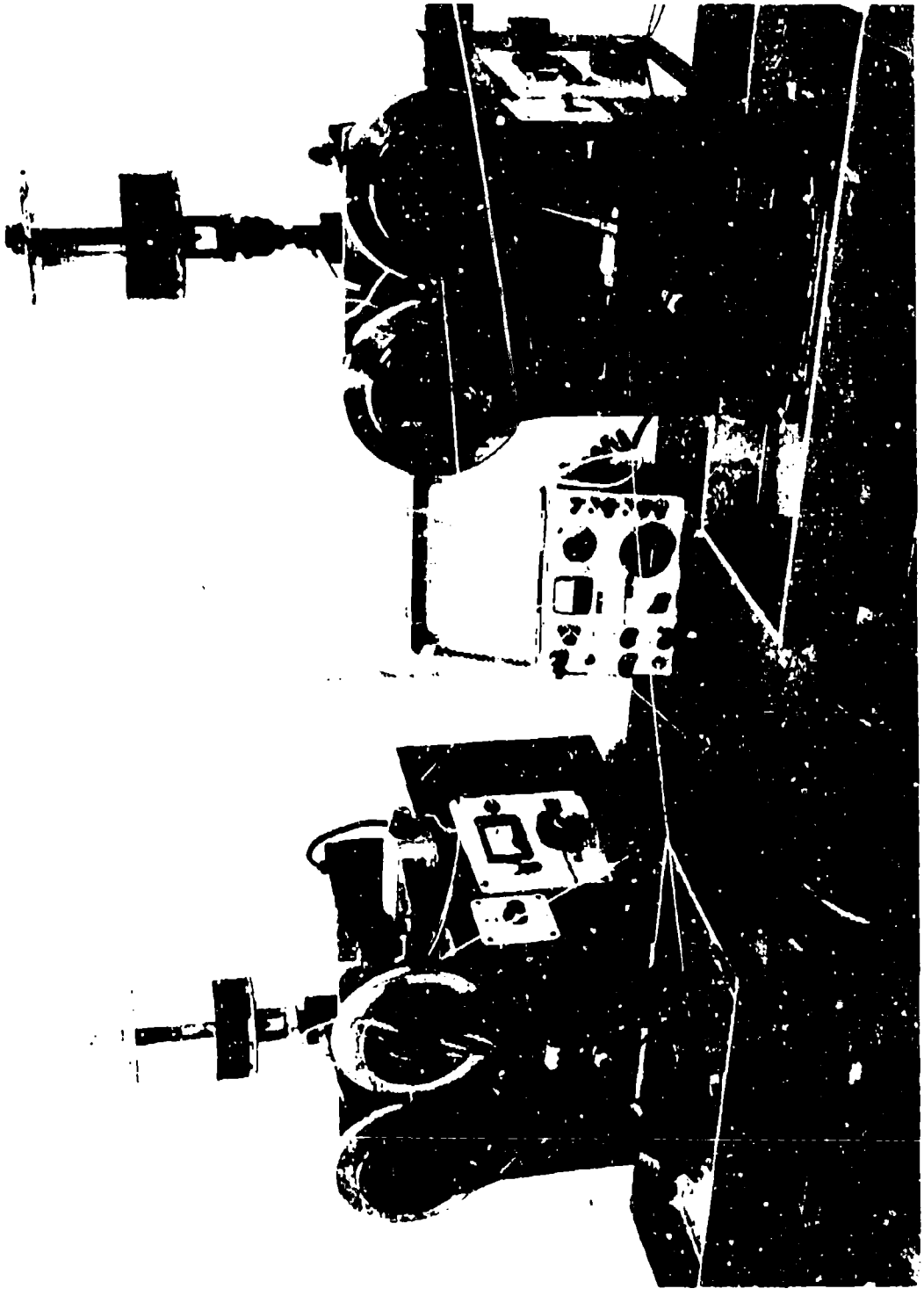

FIGURE 1 - Rolling Contact Fatigue Test Machines

Load:	69 lbs. to 325 lbs
Temperature:	70°F to 80°F
Speed:	10,000 rpm
Lubricant:	Humble Enco 2380 Type 11 Turbo Oil (MIL-L-23699B)
Specimen Geometry:	0.375 ±0.0002" diameter x 3" long. Surface finish less than 4 rms. Roundness within 100×10^{-6} inches.

2. Material Preparation - All RCF specimens were sliced from larger hot pressed billets and machined round with exception of the AD999 which was purchased in the finished geometry.

Three types of finishing procedures were used on RCF test specimens in the program to bring them to the surface finish and dimensions required.

The procedures employed are as follows:

(1) The RCF rods are roughed out from square bars between centers using a 100 grit diamond wheel (ASC100S-R75B69 specification). Then a 320 grit diamond wheel (ASD320-N75B69 specification) is used to finish to final dimensions.

Machine conditions employed are; wheel speed 5500 sfpm, work speed 600 rpm, and traverse speed 0.001 inch per revolution. Both operations are done with a fluid coolant and grinding aid (Norton Wheelmate #203 which is a rust inhibitor soluble oil).

Careful control of finish stock removal rate (0.0005 inch per pass) brings the surface finish down to between 5 and 8 micro-inch finish.

Final finish is achieved by hand lapping at 200 sfpm with a leather lap charged with 6 micron diamond paste to produce less than 5 micro-inch surface finish. Rods finished by this method have an FM prefix in the numbering sequence.

(2) The second procedure eliminates the 320 grit diamond grind of the first procedure and substitutes a mechanical lapping system to achieve final dimensions, roundness, and micro-inch finish. The mechanical lap was constructed for the purpose and utilizes a twelve specimen slotted carrier disc between two approximately twelve inch diameter cast iron horizontal lap discs. The bottom disc rotates about a fixed axis but the top disc has an oscillating axis to produce a more heterogeneous scratch pattern.

The top disc is also counterbalanced to achieve very light loading on work pieces.

The carrier slots position the specimen rods in the rotating disc at a slight angle to the radii.

The cast iron laps are charged with 6-8 micron diamond paste.

This system achieves excellent surface finish and dimensional tolerances. Silicon nitride rods produced in this manner were round to within 25 x 10^{-6} inches, were uniform in diameter to within 15 x 10^{-6} inches and had a finish of 2.5 micro-inches or better. Rods finished by this procedure have a single numbering sequence.

(3) The third procedure involves either #1 or #2 plus a burnishing step with a silicon carbide wheel and a maximum stock removal of 0.001 inch.

This last procedure was carried out to assess the feasibility of eventually utilizing a silicon carbide wheel to apply the crown to the ceramic rollers in the full roller bearing as a formed diamond wheel cannot be made or trued to the accuracy required.

3. Results - The bulk of the screening phase RCF testing on silicon nitride was carried out at the same loading 325 pounds, as for the M-50 control. Because of differences in elastic moduli, this load will induce a maximum calculated Hertz stress of 700,000 psi when steel is tested and 800,000 psi when silicon nitride is tested.

Table III gives the results for the hot-pressed silicon nitride. Densities and three-point flexural strengths taken on billets from which the rods were cut are also included. Chemical analysis and hardness of several rods is given in Table IV. The HS-110A and Lucas materials show the best fatigue properties. A Weibull distribution of 26 out of the 30 total tests for HS-110A is shown in Figure 2. Four data points were eliminated due to faulty steel test wheel geometry measured at the test completion. The Weibull plot shows the HS-110A to have nearly three times the L_{10} fatigue life of M-50 CVM steel at the same load but with 100,000 psi higher Hertz stress. The ninety percent confidence bands for each material are included in Figure 2.

HS-110B performed poorly perhaps due to material inconsistency. As this material was produced by a discontinued processing variant no extensive analysis of the failure mechanism was attempted.

HS-110C performed creditably giving lives similar to the M-50 control. The HS-130 rod, FM-11, gave a similar life. However, the results on rods #9 and #10 which had the second finishing procedure gave poor or inconsistant performance. This effect was encountered on other rods indicating that this finishing procedure was detrimental to rod life. Consequently the results from rod FM-11 are taken as more representative of HS-130 performance.

TABLE III

Rolling Contact Fatigue Life
Hot Pressed Si_3N_4

Material Designation	Rod Number (Density gm/cc) (Flexural Strength psi)	Test Load lbs	Calc Hertz Stress psi	Life 1000 cycles	Median Life 1000 cycles (L_{50})
M-50 CVM control	-	325	700,000	Results of 34 tests	3,660
HS-110A	FM-4[1] 3.15 gm/cc	325	800,000	80,335[S]	30,650
				20,061	
				16,509	
				16,800	
				37.397[S]	
	FM-5 3.15 gm/cc	325	800,000	52[3]	
				35,468	
				34,949[S]	
				56,658[S]	
				41,899[2S]	
				49,782[2S]	
				37,316	
				10,492	
	FM-6 3.15 gm/cc	325	800,000	31,977	
				9,405[2S]	
	FM-10 3.11 gm/cc 112,359 psi	325	800,000	457[3W]	
				1,092[3]	
				306[3Wn]	
				20,813	
				47,921[S]	
				29,806[S]	
				51,704[S]	
				23,926[S]	
				22,600	
				2,868	
				1,207	
				13,631	
				10,877	

1. Unless noted rods finished by procedure #1
2. Test wheels failed
3. Values not used in weibull plot
4. Rod finished by procedure #1 except final lapping omitted
5. Rod finished by procedure #2

s -denotes suspended test
w - " wheels qualified
wn - " wheels not qualified

(continued)

TABLE III (continued)

Material Designation	Rod Number (Density gm/cc) (Flexural Strength psi)	Test Load lbs	Calc Hertz Stress psi	Life 1000 cycles	Median Life 1000 cycles (L_{50})
HS-110B	FM-3 3.18 gm/cc 122,688 psi	325	800,000	650 60 418 12,603 5 7 6 100	80
HS-110C	FM-7 3.20 gm/cc 138,571 psi	325	800,000	225wn 4,100 4,729 1,770 28,218	4,553
	FM-8 3.20 gm/cc 138,571 psi			15,247 3,576 6,273 4,377	
Lucas	FM-14	325	800,000	34,065 55,411	
HS-130	FM-11 3.19 gm/cc 130,881 psi	325	800,000	5,119 44wn 2,968 14,468 4,334 49,871s	5,119
	9[s] 3.18 gm/cc 137,400 psi	325	800,000	9,170 147 110 094 132	132
	10[s] 3.18 gm/cc 137,400 psi	325 220 220 220 220 150 150	800,000 700,000 700,000 700,000 700,000 610,000 610,000	365 7,742 461 2,706 660 46,237s 44,751s	

TABLE IV

Chemical Analyses and Hardnesses

Rod Identity	Elemental Composition(%)				DBH_{300} (kg/mm^2)
	Al	Fe	Ca	Mg	
FM-1	0.74	0.44	0.20	0.50	2282
FM-4	0.60	0.46	0.36	0.76	2350
FM-10	0.62	0.42	0.26	0.73	2304
FM-11	0.22	0.30	0.12	0.66	2337

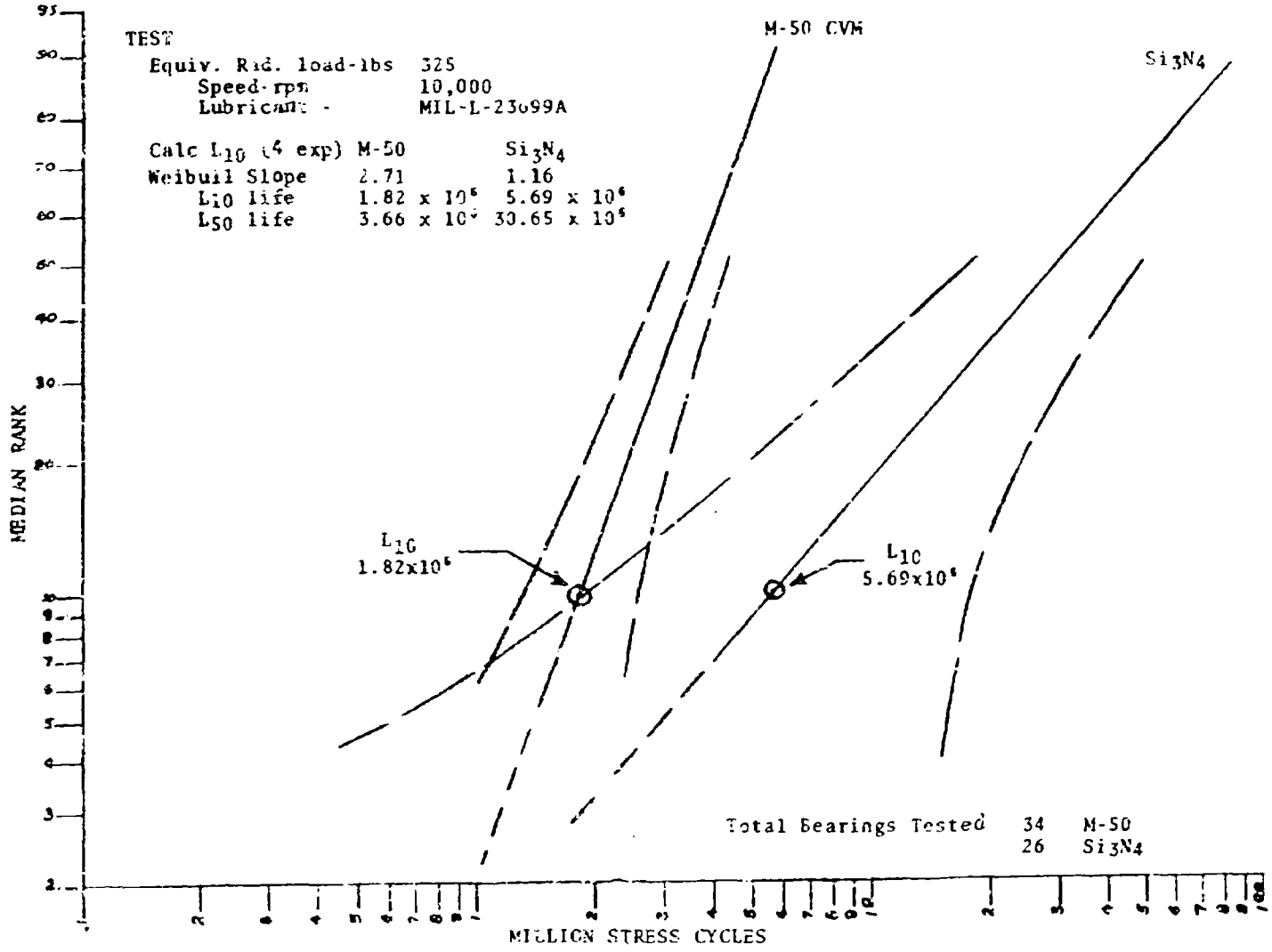
TEST
Equiv. Rad. load-lbs 325
Speed-rpm 10,000
Lubricant - MIL-L-23699A
Calc L_{10} (4 exp) M-50 Si_3N_4
Weibull Slope 2.71 1.16
L_{10} life 1.82×10^6 5.69×10^6
L_{50} life 3.66×10^6 30.65×10^6
M-50 CVM
Si_3N_4
L_{10} 1.82×10^6
L_{10} 5.69×10^6
Total Bearings Tested 34 M-50
26 Si_3N_4
MEDIAN RANK
MILLION STRESS CYCLES

FIGURE 2

An important observation in all the fatigue testing of silicon nitride is that it fails by spalling and not by catastrophic means as might be expected of a brittle material. Figure 3 shows a spalled silicon nitride rod and a spalled steel rod showing the similarity in failure spalls.

Figure 4 shows a typical silicon nitride spall under higher magnification.

The results for RCF testing of silicon carbide and aluminum oxide are given in Table V. In this case the silicon carbide RCF rods were finished by procedure #2 while the aluminum oxide rods as purchased had a 2.5 microinch finish. No further finishing was done on these rods and the details of the supplier's procedure is unknown.

Since both silicon carbide and aluminum oxide have moduli of elasticity well above 50 million, significantly lower loads were required to produce Hertz stresses comparable to those under which the steel and silicon nitride were tested. Even at these reduced loads and stresses silicon carbide produced relatively short lives with frequent rod fractures. The only attempt at 800,000 Hertz stress resulted in almost immediate catastrophic fracture. Although these results could probably be improved by the use of finishing procedure #1 it is felt unlikely that this would raise the performance level to that of silicon nitride.

The aluminum oxide tests were generally suspended due to crushing in the ceramic contact area. Figure 5 shows a linear proficorder chart of aluminum oxide rod #1 across the contact area. Note the deep groove caused by the crushing. Compare this trace with that across an M-50 steel specimen shown in Figure 6. Because of this crushing encountered at light loads no attempts were made to run aluminum oxide at 800,000 psi Hertz stress.

As a result of these tests HS-110A silicon nitride was chosen as the principal material candidate for further environmental testing and for fabrication into bearing rollers for the full scale bearing test. Some further environmental testing was also carried out on the silicon carbide however.

B. FOUR BALL TESTING

1. Description of Equipment - A small number of four ball tests on silicon nitride were performed as part of the screening program. These were run on a Federal-Mogul test unit shown in Figure 7 and shown schematically in Figure 8. This unique design employs three Federal-Mogul Westwind air bearings to eliminate external friction and vibration and to insure contact of the test ball with all three slave balls. Maximum Herts contact stresses (calculated for non-lubricated conditions) for the tests performed varied from 615,000 psi to 780,000 psi.

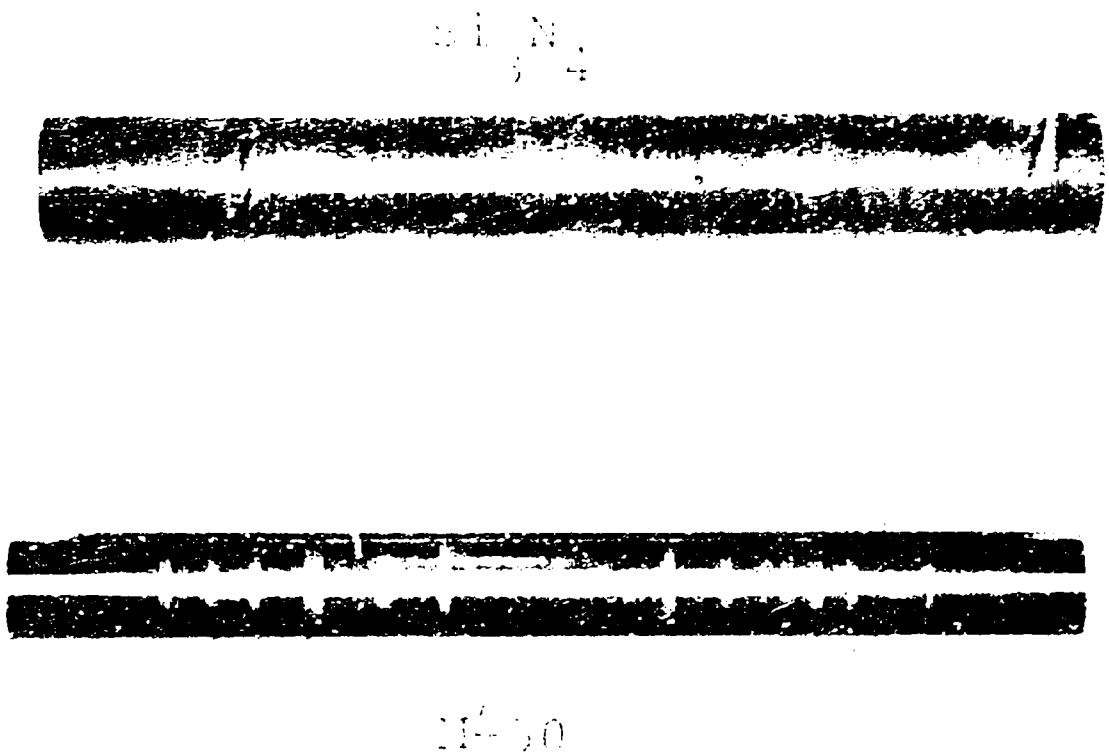

FIGURE 3 - Silicon Nitride and M-50 Rods Showing Similarity of Fatigue Spalls

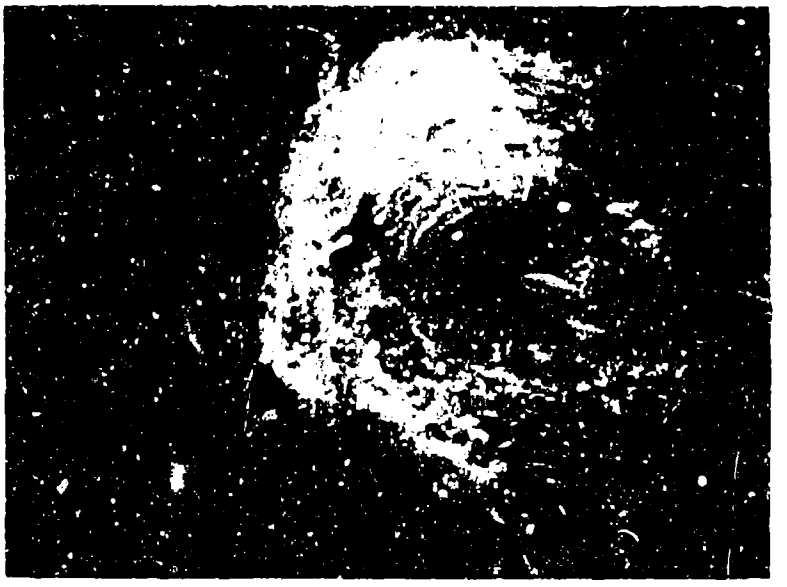

FIGURE 4 - Spall in Silicon Nitride Rod #FM-5
(Norton Material DM)
Life - 10.492 x 10^6 Cycles
Magnification - 80X

TABLE V

Rolling Contact Fatigue Life
Hot Pressed SiC and Dense Sintered Al_2O_3

Material Designation	Rod Number (Density gm/cc) (Flexural Strength psi)	Test Load lbs	Calc Hertz Stress psi	Life 1000 cycles	Comments
SiC HX-294	5	109	600,000	779	
	3.20 gm/cc	109	600,000	6,319	
	128,296 psi	170	700,000	10,853	
		170	700,000	4,706	
	6	109	600,000	1,235	
	3.20 gm/cc	109	600,000	4,130	
	128,296 psi	170	700,000	4,186	
		170	700,000	2,674	
		225	800,000	<1	rod fractured during test
	0	109	600,000	20,205	suspended
		109	600,000	24,270	suspended
		170	700,000	17,718	suspended fractured upon removal
	2	170	700,000	966	suspended fractured during test
Al_2O_3 AD999	1	69	500,000	27	suspended
		69	500,000	44	suspended
		69	500,000	33,730	suspended
		120	600,000	46,195	suspended
	2	120	600,000	4,326	
		120	600,000	1,631	
		190	700,000	714	suspended

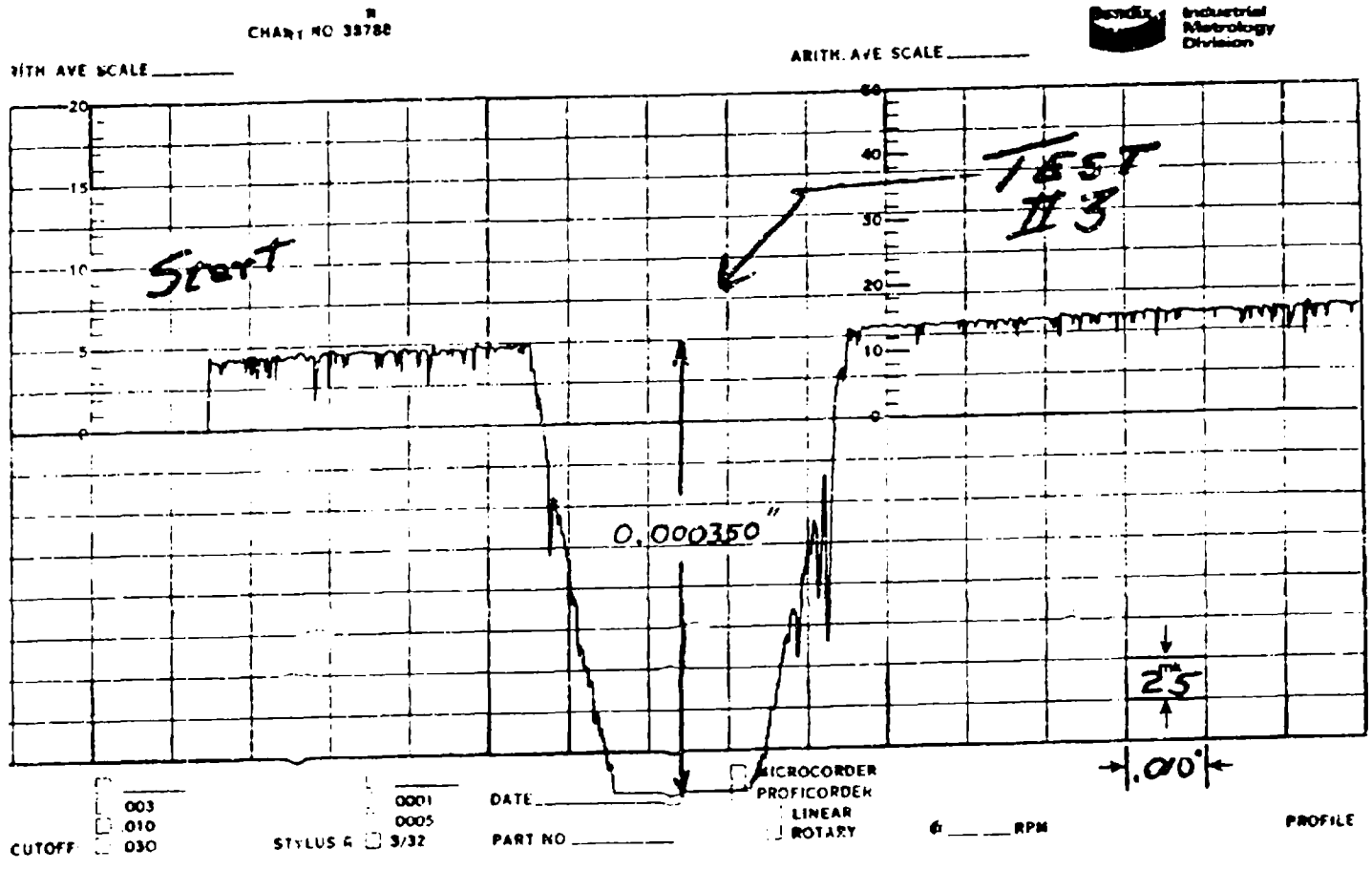

69 Pounds Load, 500M PSI Hertz Stress

FIGURE 5

Linear Proficording Across Test Track on AD999 Aluminum Oxide Bar #1

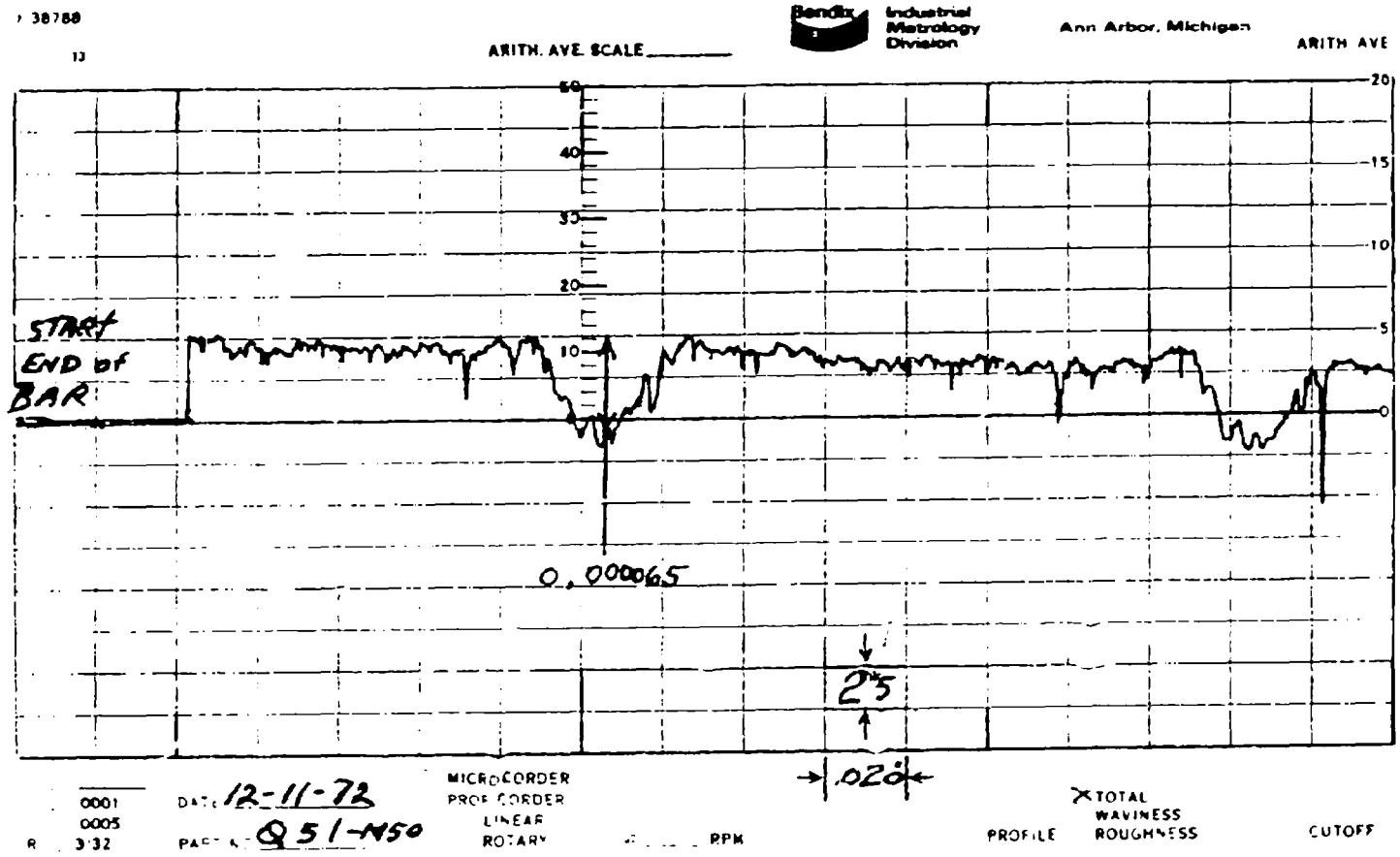

325 Pounds Load, 700 MPSI Hertz Stress

FIGURE 6

Linear Proficording Across Test Tracks on M-50 CVM

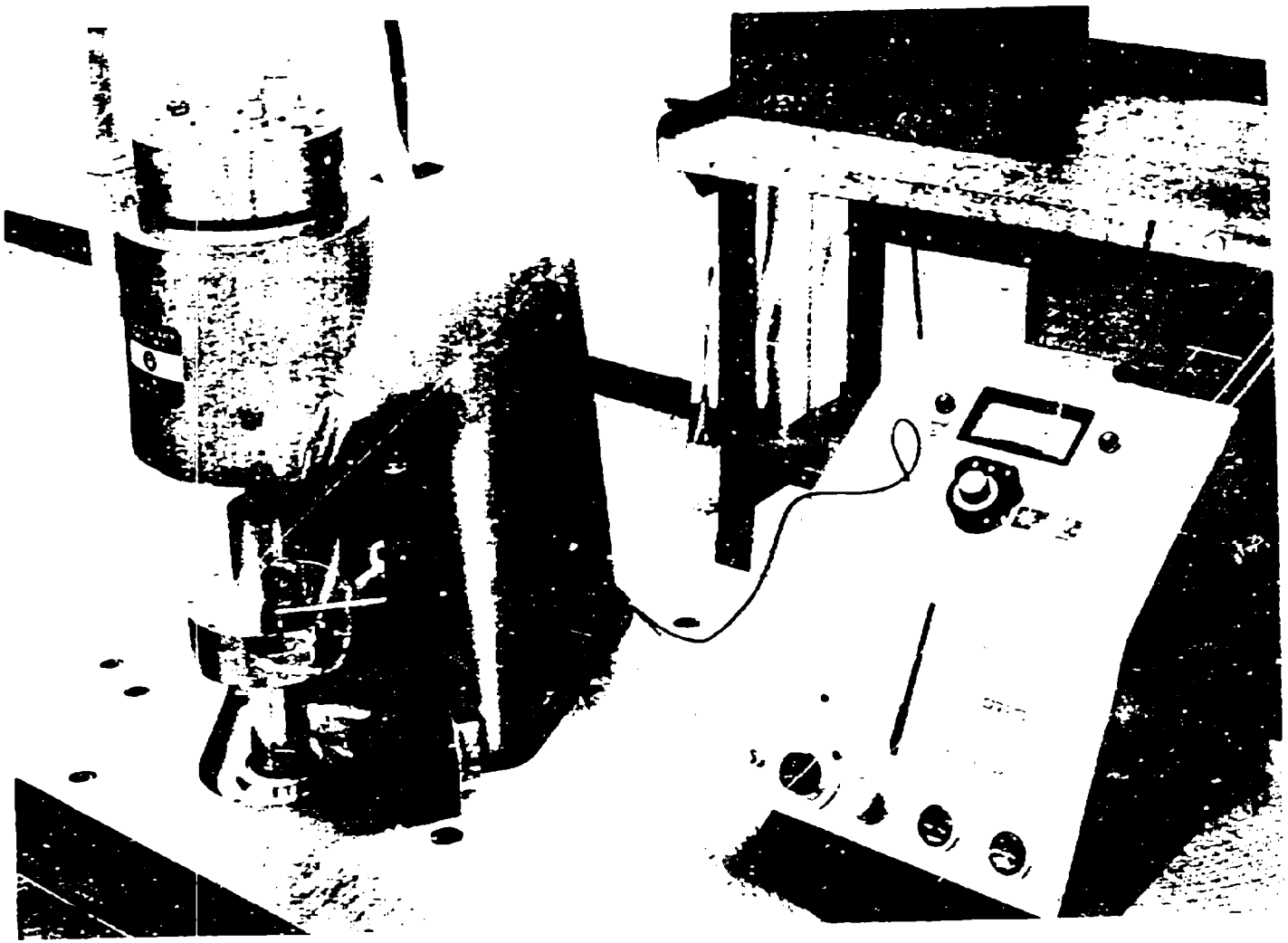

FIGURE 7 - Federal-Mogul Four Ball Test Machine

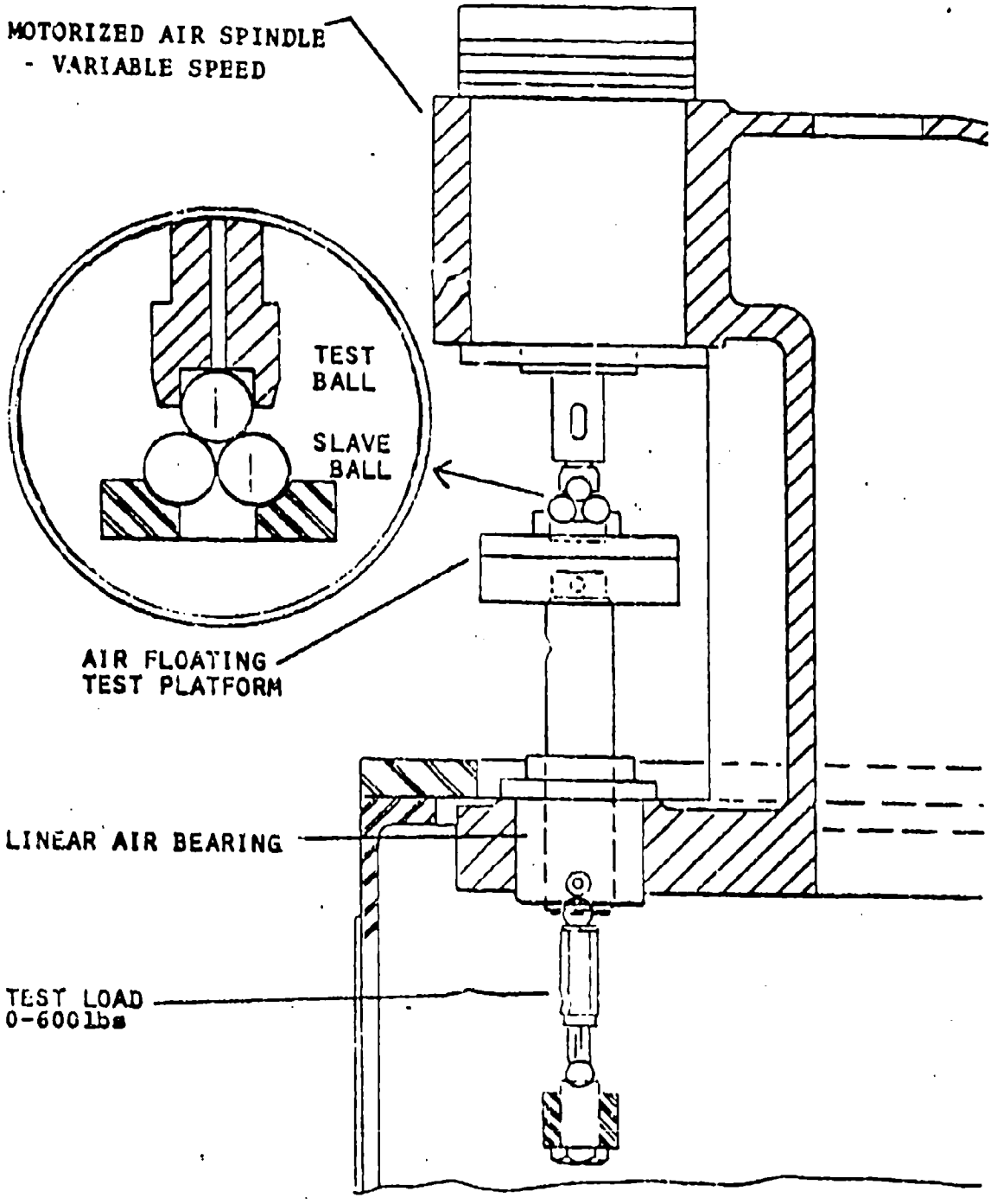

FIGURE 8 Schematic of the Four-Ball Tester

2. Material Preparation - Balls tested were fabricated from a single billet of HS-110B having a mean flexural strength of 107,917 psi and a density of 3.19 gm/cc. The billet was sliced into 5/8 inch cubes with diamond cut-off wheels and finished into balls at Industrial Tectonics Inc., Ann Arbor, Michigan, by a proprietary ball making process. Finished condition of balls was requested and received as follows:

(A). Requested - AFBMA Grade 10 1/2" diameter nominal

Surface Roughness Tolerance 1.0 microinch "AA"
Out-of-Roundness, Maximum 0.000010"

(B) Received

Surface Roughness 1.1 - 1.5 microinch "AA"
Out-of-Roundness, Typical 0.000020"

3. Results - The four ball test results shown in Table VI are generally poor and inconsistent when compared to all steel balls. M-50 and 52100 balls have a life range of 100 to 500 hours at a calculated Hertz contact stress of 780,000 psi. In two cases, test numbers 8 and 10, more encouraging results were obtained on a different contact area of a ball which had previously worn badly. Several reasons for the inconsistency and poor life can be postulated. These balls were taken from billets of HS-110B, a material which gave erratic RCF test results, Table III. The geometry of the balls was not to Grade 10 specifications. Proficorder checking of the out of roundness showed wide variations in excess of Grade 10 specifications. The surface finish in addition to being outside the Grade 10 specification showed extensive pitting, Figure 9.

For these reasons it is felt that this testing does not represent the results that would be obtained from silicon nitride under normal conditions.

C. FRICTION AND WEAR TESTING

The test machine used for wear testi determining the coefficients of sliding friction was the A-6 unit shown in Figure 10.

This unit employs the ring and flat concept resulting in a line contact between the two test com s. The rings are 1.3775" OD by 0.3437" wide and the blocks 0 x 0.4" x 0.250".

Test conditions were as follows:

1. Materials: Silicon nitride HS-110A
Silicon carbide HX-294
AISI 8620 and M-50 CVM

TABLE VI

FOUR-BALL TEST RESULTS

Test Number	Test Ball (Ball Number)	Slave Balls	Load Pounds	Hertz Stress 10^3 psi	Life Hours	Spall	Wear Track
1.	Si_3N_4 (0)	52100	145	780	80.6*	No	160×10^{-6} deep**
2.	52100	1 Si_3N_4 (1) 2 52100	145	780	28.1	Si_3N_4	---
3.	Si_3N_4 (2)	Si_3N_4 (3,4,5)	100	780	8.6	Test Ball	---
4.	Si_3N_4 (2) (different contact area)	Si_3N_4 (3,4,5)	100	780	1.5	Slave Ball	---
5.	Si_3N_4 (6)	M-50	145	780	0.6	Test Ball	
6.	Si_3N_4 (6) (different contact area)	M-50	145	780	29.6*	--	deep**
7.	Si_3N_4 (7)	M-50	105	690	100.0*	--	110×10^{-6} deep**
8.	Si_3N_4 (7) (different contact area)	M-50	105	690	97.2*	--	20×10^{-6} deep
9.	Si_3N_4 (8)	M-50	75	615	113.1*	--	deep**
10.	Si_3N_4 (8) (different contact area)	M-50	75	615	113*	--	very slight

*Suspended **Dark contaminant noted in lubricant after commencement of test.

500 SEM

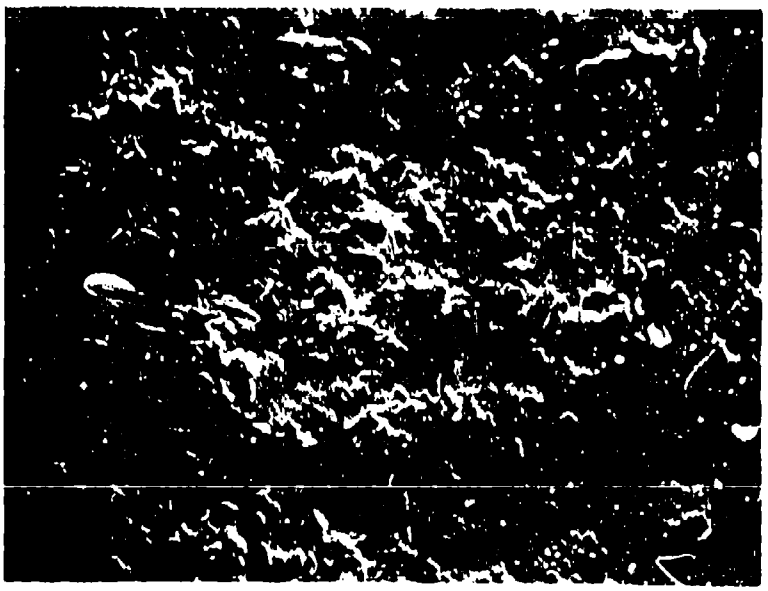

2000X SEM

FIGURE 9 - Surface of Silicon Nitride Ball

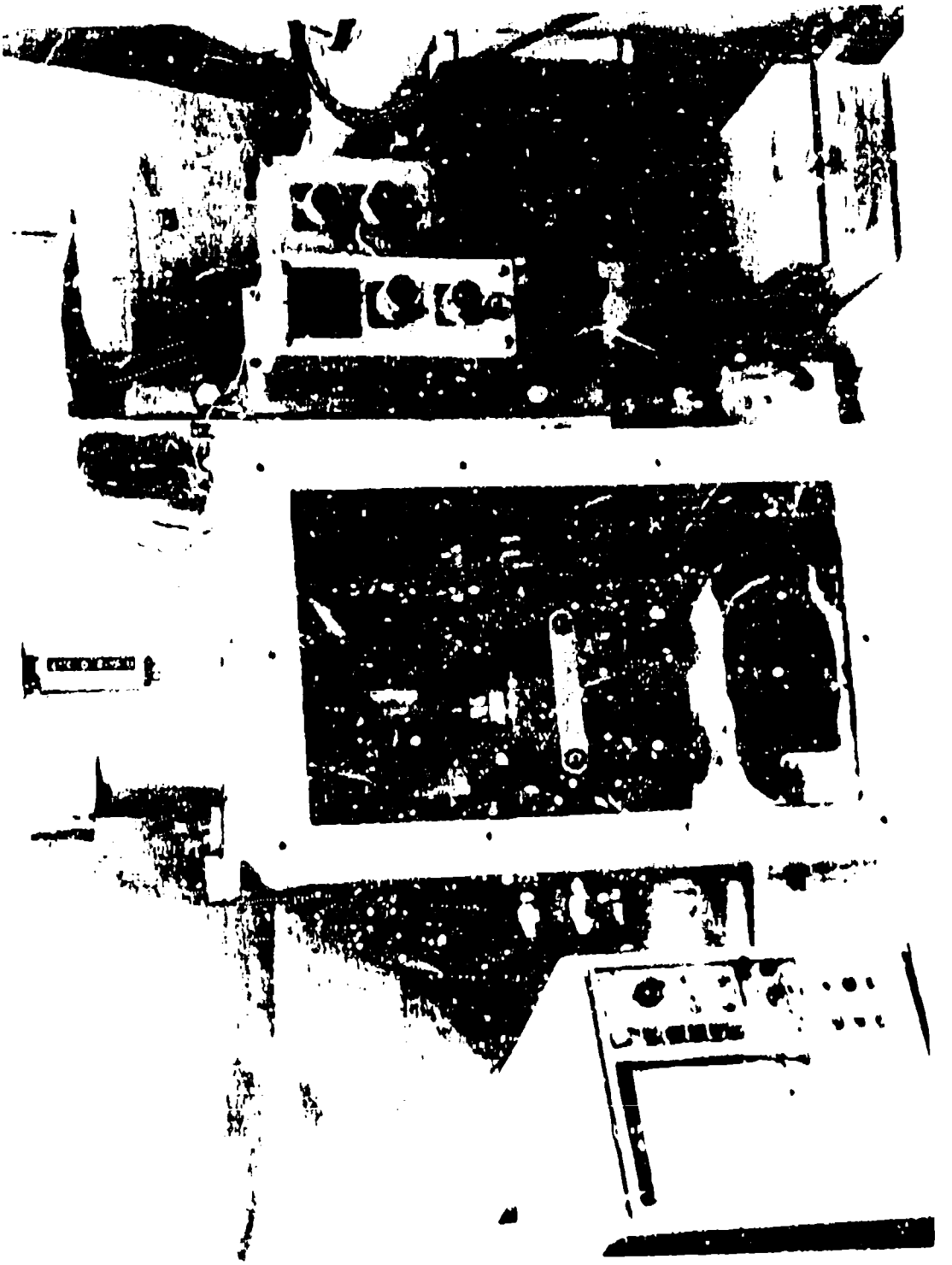

FIGURE 10 - Hohman A-6 Wear Test Machine

2.	Lubrication:	Enco 2380 Type II Turbo Oil (MIL-L-23699B)
3.	Temperature:	75°C at start of test
4.	Load:	50 pounds
5.	Speed:	800 rpm
6.	Length:	5,000 revolutions

The test combinations and the results are given in Table VII. The coefficients of friction were determined from the frictional force after 2,000 revolutions and the widths of the wear scars were measured after 5,000 revolutions.

Examination of the results shows that, in general, steel in contact with silicon nitride or silicon carbide produces less wear and a lower coefficient of friction than when two ceramics are in contact. This is shown particularly when comparing silicon nitride with itself and with steel. Test 9 again displayed the brittleness of silicon carbide when the ring cracked during the test. The excessive wear scar width of 0.044 inch is due to the crack "knife edge".

Comparing silicon nitride versus steel with steel versus steel, it is seen from the table that the average coefficients of friction for both combinations is 0.15. Although the wear width scars for steel versus steel are slightly lower than for steel versus silicon nitride the magnitudes are such that excessive wear should not be encountered in a full scale bearing with silicon nitride rollers.

D. ENVIRONMENTAL TESTING

1. Dimensional Stability - Bearing steels, especially those which received an improper heat treatment, tend to change size when subjected to cyclic temperatures. This change can affect the dimensional characteristics of the bearing, especially the diametral clearance and the amount of interference fit on the shaft. Silicon nitride and silicon carbide were cycled from -65°F to 450°F to measure their stabilities. A total of eighty cycles was performed with M-50 CVM steel also for reference. The measurements are tabulated (Table VIII) showing no detectable dimensional changes for silicon nitride and silicon carbide. The M-50 CVM did have a slight size change of +10 millionths of an inch in five inches.

The set up for measurement of the five inch long rods is shown in Figure 11. Through the use of multiple master bars, accuracy is $\pm 5 \times 10^{-6}$ inches in the five inches.

2. Effects on Fatigue Life by Salt Water and Hot Type II Turbo Oil - To determine if silicon nitride or silicon carbide would be chemically attached by typical bearing environments during long term exposure, both materials were exposed to hot lubricant and a warm salt solution for a several week period.

TABLE VII

Wear Test Results at 50 Pounds Load and 75°F

Test #	Materials Ring	Materials Blocks	Measured Coefficient of Friction @2000 Cycles	Wear Scar Width @ 5000 Cycles	Remarks
1	Steel (8620)	Si_3N_4	0.16	0.017"(1)	
2	Steel (8620)	Si_3N_4	0.17	0.018"	
3	Steel (8620)	Si_3N_4	0.12	0.018"	
4	Steel (8620	Si_3N_4	0.13	0.019"	
5	Steel (8620)	SiC	0.15	0.015"	oil black
6	Steel (8620)	SiC	0.15	0.014"	oil black
7	Si_3N_4	Si_3N_4	0.20	0.021"	
8	Si_3N_4	Si_3N_4	0.19	0.022"	
9	SiC	SiC	--	0.044"	ring split
10	SiC	SiC	0.15	0.028"	
11	Si_3N_4	SiC	0.20	(2)	ring cracked
12	Steel (8620)	Steel (M-50)	0.15	0.016"	
13	Steel (8620)	Steel (M-50)	0.15	0.016"	
14	Steel (8620)	Steel (M-50)	0.15	0.016"	

(1) - Wear width @ 10,000 cycles
(2) - Ring cracked at 3,975 cycles - uneven scar

TABLE VIII

Dimensional Stability of Silicon Nitride and Silicon Carbide Compared to M-50 CVM

Rod Number	Number of Cycles(1) 0	12	28	80
	Millionths of an inch change from initial measurement(2)			
M-50 (1)	0	+3	+7	+10
M-50 (2)	0	+2	+4	+6
Si_3N_4 (1)	0	-1	-1	-1
Si_3N_4 (2)	0	0	0	0
SiC (1)	0	-1	-1	-1
SiC (2)	0	0	-1	-1

(1) Bars cycled as follows:

A. 1 hour 450°F)
B. 1 hour -65°F) 1 Cycle
C. Repeat A and B

(2) Millionths of an inch in five inches.

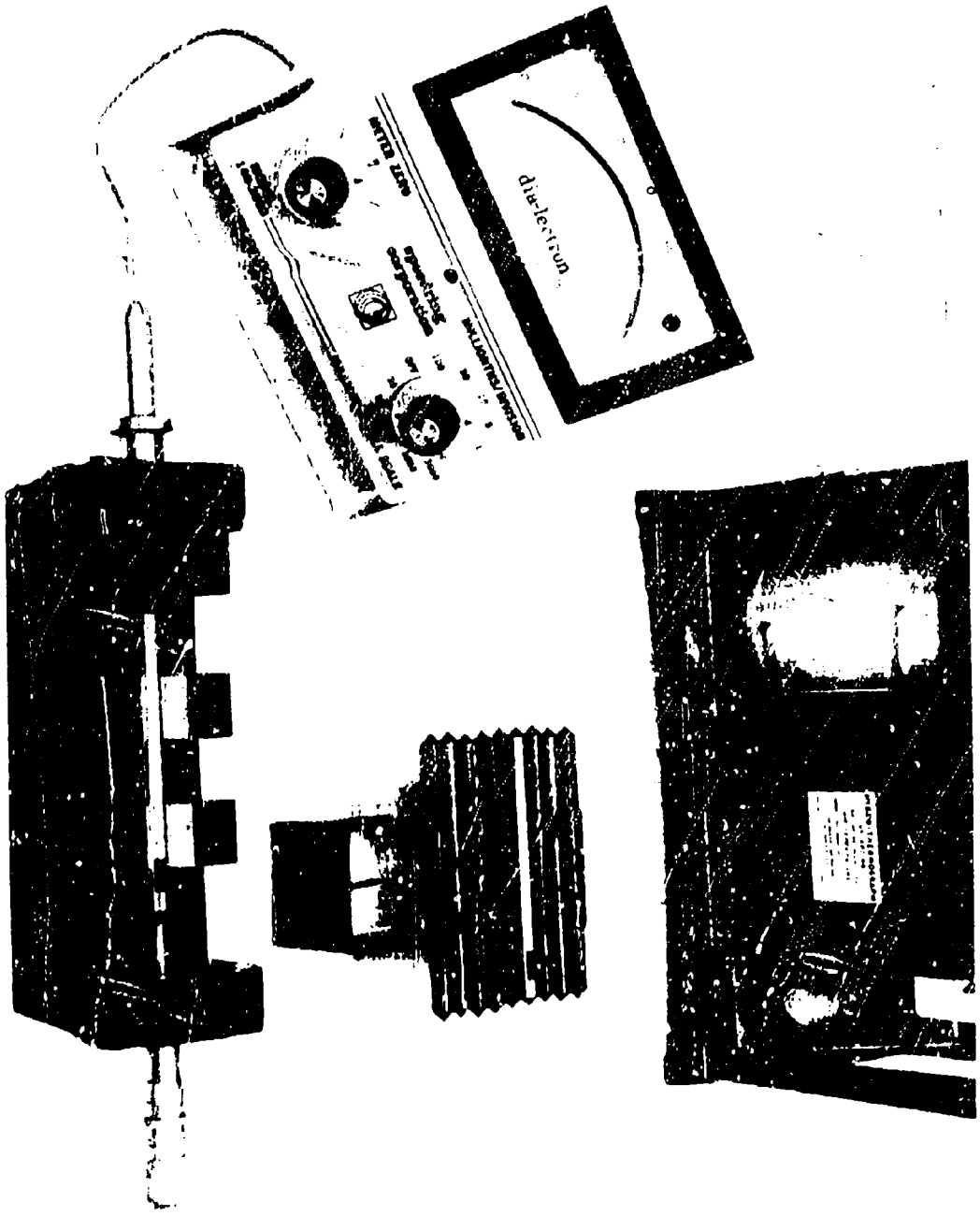

FIGURE 11 - Dimensional Stability Measurement Set-Up
Accuracy of ±0.000005"

RCF rod #19 made from HS-110A silicon nitride was fatigue tested initially, photographed, weighed and exposed to Enco 2380 Turbo Oil for three weeks at 450°F. At the end of the exposure the rod was re-weighed, photographed and subjected to three additional fatigue tests. The rod did not change in appearance or weight, indicating inertness to the environment. The fatigue tests results were inconclusive (Table IX) due to the short duration of the initial tests. This was typical for rods finished by procedure 2 which unfortunately was used for all rods tested in this section.

RCF rod #22 made from HS-110A silicon nitride was fatigue tested initially, photographed, weighed and exposed to a 3.5 percent sodium chloride solution at 200°F for three weeks. At the end of the exposure, the rod was again weighed, photographed and tested. The rod did not change in appearance or in weight, indicating it did not react with the salt solution. As can be seen in Table IX the fatigue life again was low and inconsistent before and after exposure.

3. Lubricant Shut Off and Entrained Particles - HS-110A silicon nitride rod #21 was run for two tests initially then for one test with the lubricant shut off after starting. The results are shown in Table IX. Although no catastrophic or varying failure modes occured without lubrication, the results are inconclusive due to the short duration of the initial tests.

Rod #21 was also tested with an abrasive in the lubricant. Four tests were performed with 5 micron Arizona road dust (FM AC #1543094) entrained in the Enco 2380. The results shown in Table IX are also inconclusive due to the short lives of the initial tests.

IV. FULL SCALE BEARING

A. Design

The bearing selected for testing with silicon nitride rolling elements, M-50 steel races and an AISI 4340 steel retainer is a modification of a Bower Aircraft bearing. The drawings of the races and rollers are shown in Figures 12 and 13. These are slight modifications of the original bearing incorporating the latest design criteria for high speed use. Typical engine operating conditions for the original bearing are as follows:

Load	Radial only 265# to 380#
Speed	37,000 rpm
Temperature	250°F to 400°F
Calculated Life	10,000 hours L_{10}

With the design modification and with silicon nitride rollers, the bearing is expected to perform up to 65,000 rpm.

TABLE IX

Rolling Contact Fatigue Life - HS-110A Silicon Nitride
Environmental Exposure Tests

Rod Identification	Density gm/cc	Flexural Strength psi	Load lbs	Hertz psi	Life 1000 Cycles
19	3.14	115,097	325	800,000	38
Initial Test	↓	↓			
After 3 Weeks @ 450°F in Enco 2380			325	800,000	212
			325	800,000	524
			325	800,000	113
22	3.14	117,118	325	800,000	630
Initial Test	↓	↓			
After 3 Weeks @ 200°F in Salt Water			325	800,000	116
			325	800,000	326
			325	800,000	2,645
21			325	800,000	40
Initial Tests			325	800,000	34
Lube Shut-Off			325	800,000	72
5 Micron Arixona Road Dust in Enco 2380			325	800,000	168
			325	800,000	26
			325	800,000	298
			325	800,000	260

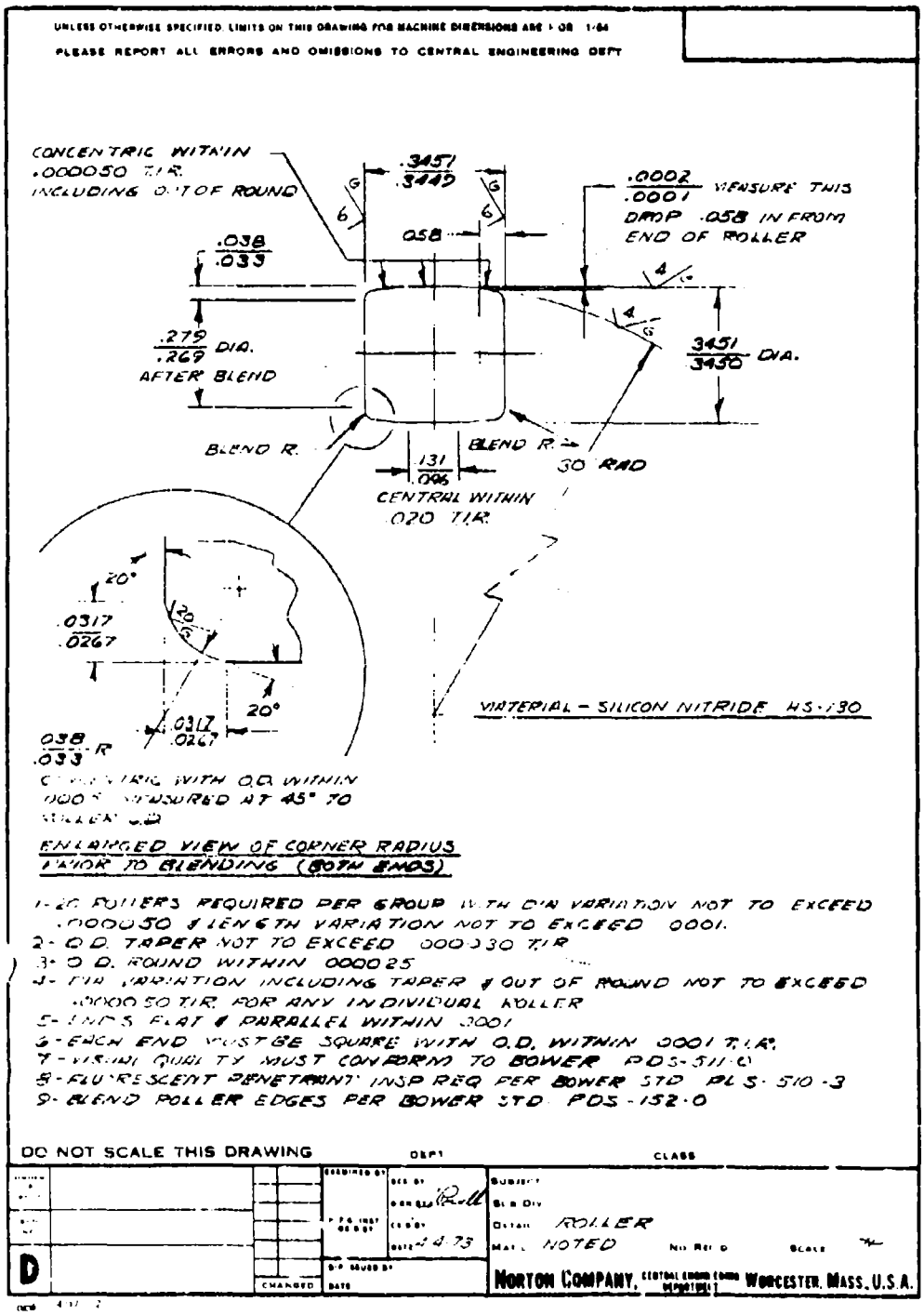

FIGURE 12 - Bearing Roller Design

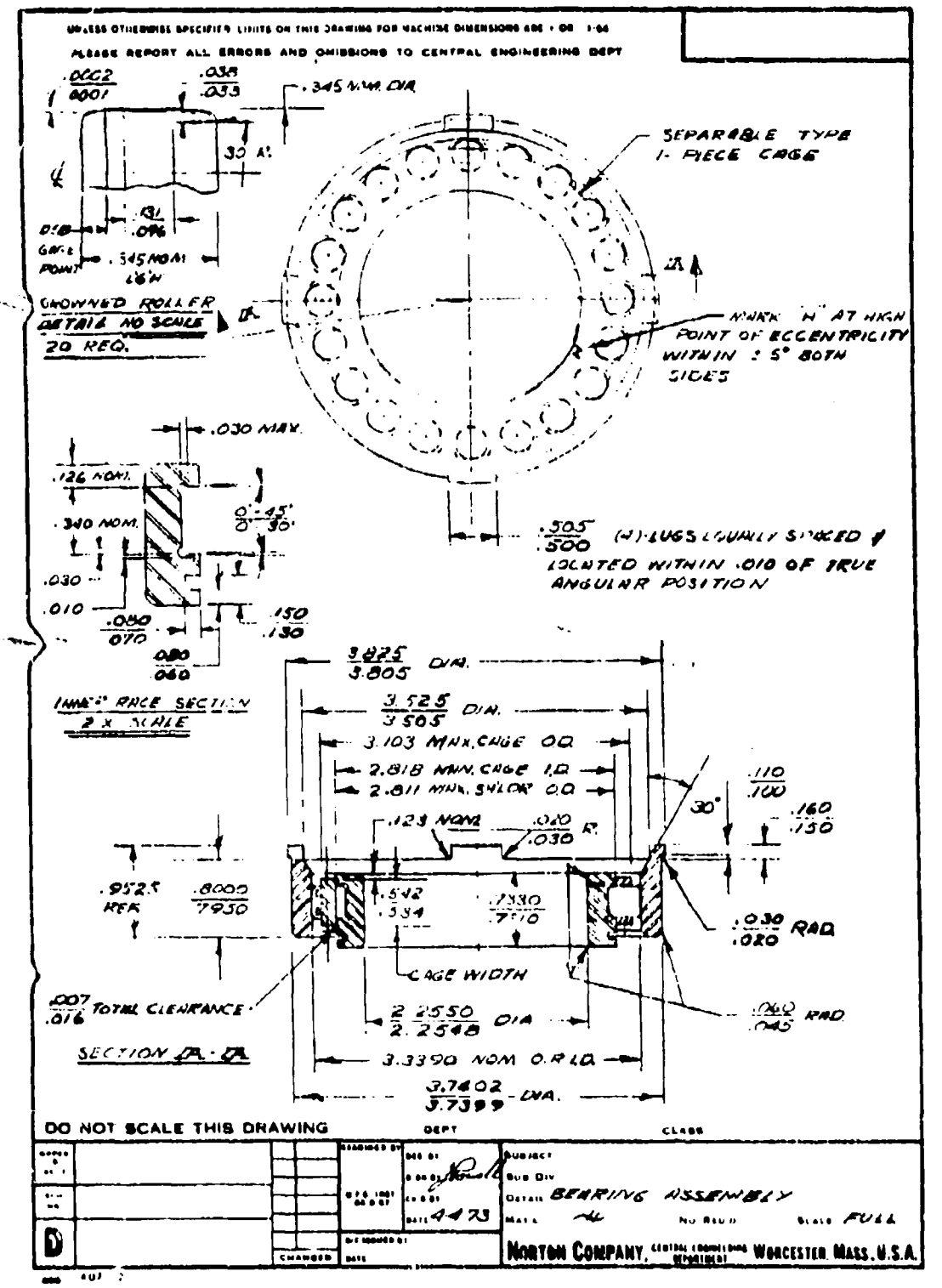

FIGURE 13 - Ceramic Bearing Assembly

Extremely close tolerences are required for bearings of this type. For instance, roller diameter variation including taper and out of round must not exceed 0.000050 inch for any individual roller in the bearing.

B. Test equipment and procedures

The test rig shown in Figure 14 will be used for the full bearing tests. In the rig, the outer race is stationary and the inner race can rotate up to 10,000 rpm with the shaft. The DN value would then be 0.5×10^6. The load will be varied during the tests and be applied radially only (maximum 4000 pounds). Lubricant will be a Type II turbo oil. Because of the relatively low rotational speed and loads, it is expected that operating temperature of the bearing will be on the order of 100°F. adaptors to hold the test bearing and support bearings for operation have been designed and fabricated. The adaptors and support bearings are pictured in Figure 15.

The test bearing is mounted on shaft (1) and placed inside of collar (2) through which the radial load is applied. The ends of the shaft are supported by conventional bearings (3).

C. Materials Fabrication

1. Metal Components

The Bearing Group of Federal-Mogul was assigned the fabrication of the races, retainers and the rollers for three complete bearings. The races and retainers made from standard aircraft bearing materials were produced without difficulty.

2. Ceramic Bearing Roller Preparation

(a) Silicon Carbide Finish Grinding - The final OD grinding and crowning of bearing rollers is conventionally done by plunge grinding using a frequently dressed silicon carbide grinding wheel. No techniques nor wheels are available to obtain the same accuracy with diamond wheels.

The effect of a final silicon carbide grinding operation upon rolling contact fatigue was checked by taking rods FM-7 and FM-8 from the initial screening study and removing 0.001 inch by silicon carbide grinding then retesting. The results are shown in Table X. The silicon carbide regrind in no way seemed detrimental, and if anything, beneficial, so this route was chosen for bearing roller finishing.

(b) Ceramic Roller Preparation - One hundred thirty HS-110A silicon nitride roller blanks were diamond ground to 0.355 inch diameter x 0.355 inch long, 0.010 inch over size for dimensions. A twenty roller sample for dimensions is shown in Table XI. The finish grinding is a three step process, (1) corner radii and rough OD, (2) end grinding and end honing, and

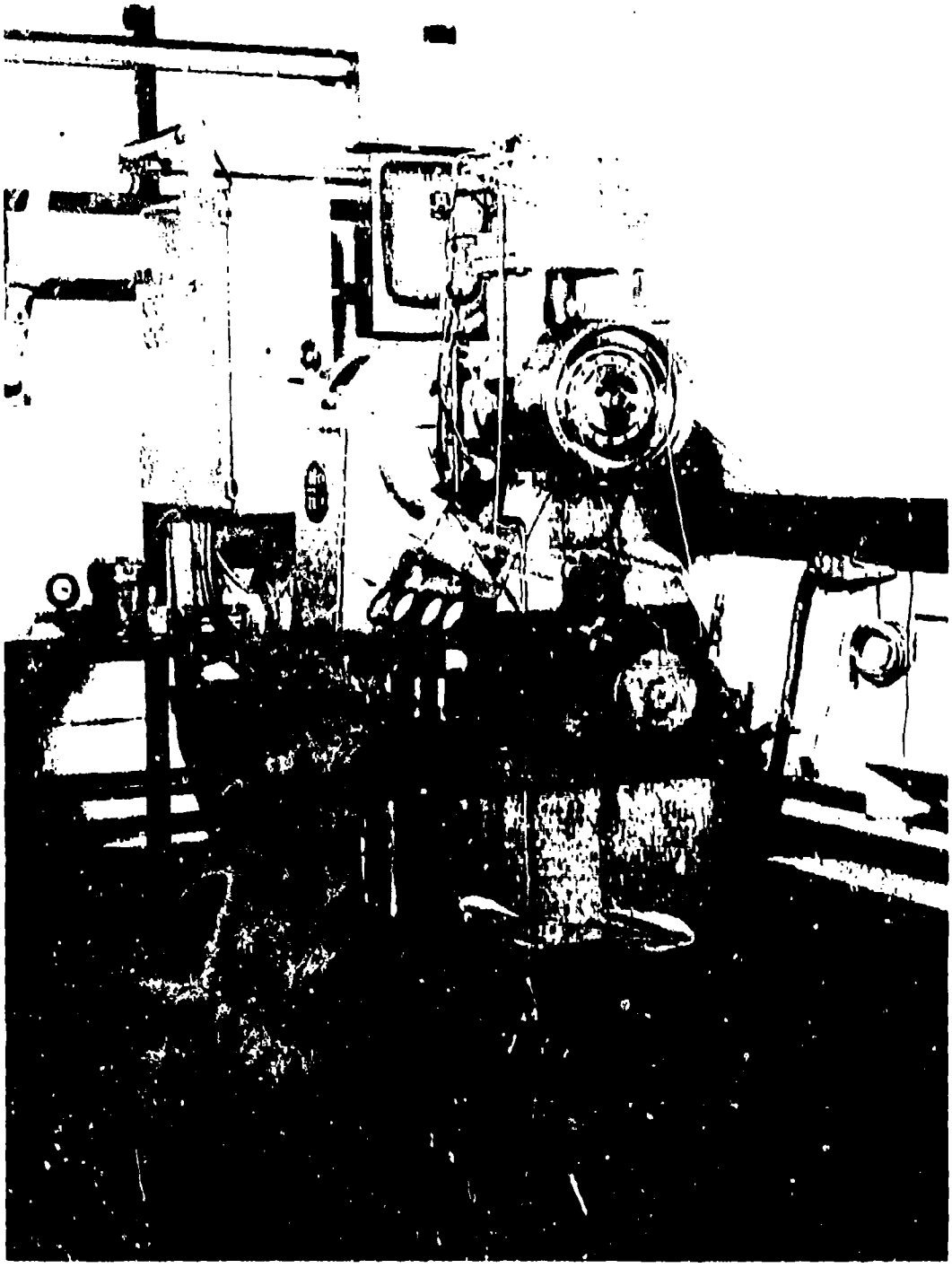

FIGURE 14 - Variable Speed Bearing Test Machine, Speed to 10,000 rpm, Loads to 4,000 Pounds

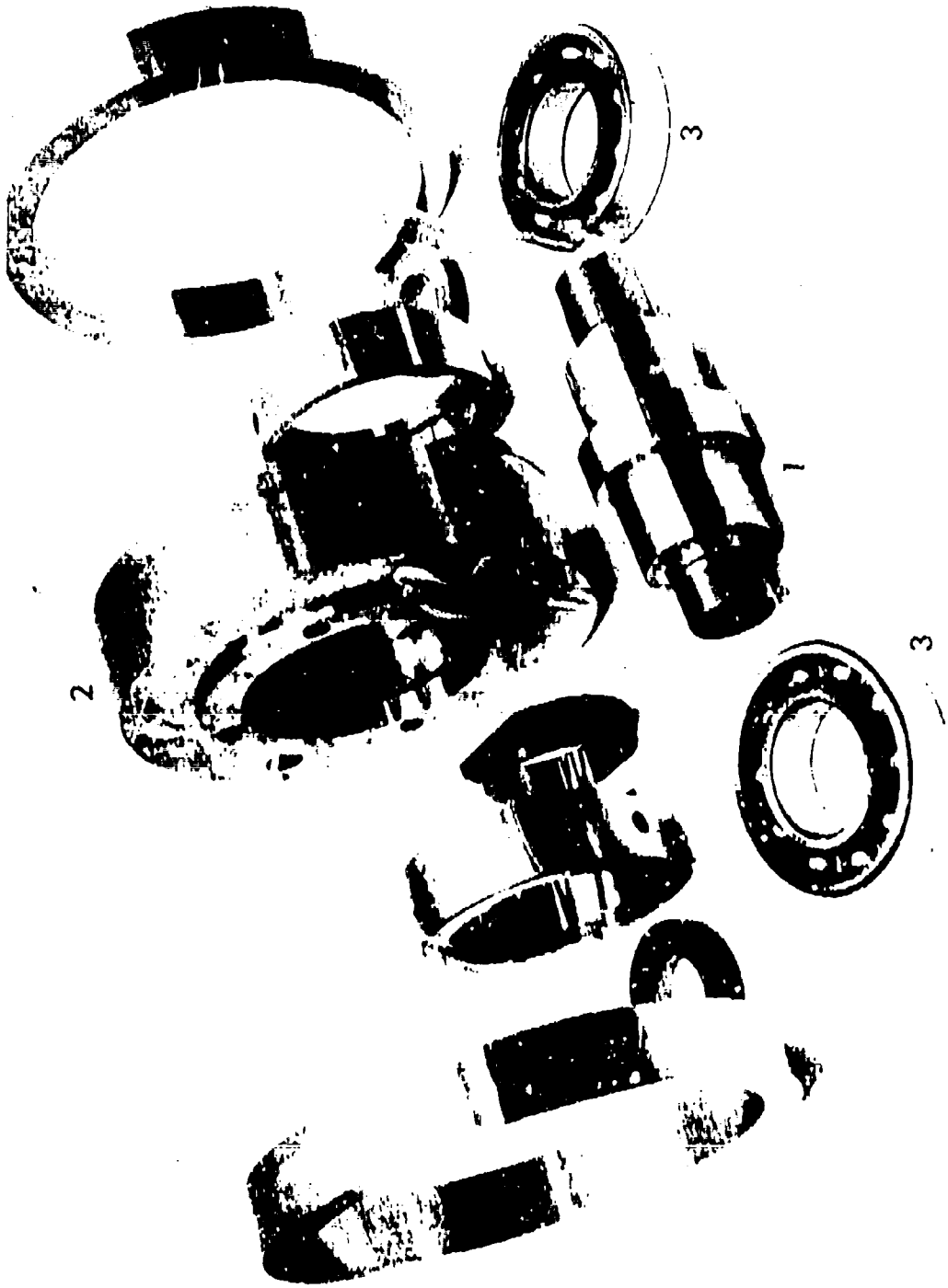

FIGURE 15 - Bearing Test Adapters and Support Bearings

TABLE X

Effect of Silicon Carbide Grinding on Fatigue Life of HS-110A Si_3N_4

Rod Identification	Load Lbs.	Calc Hertz Stress psi	Life 1000 Cycles	Median Life 1000 cycles
FM-7 As Received	325	800,000	225 N.G.	4,500
			4,100	
			4,739	
			1,770	
			28,218	
FM-8 As Received			15,247	
			3,576	
			6,273	
			4,377	
FM-7 After SiC grinding			24,711 S	24,700
			31,584 S	
			17,515	
FM-8 After SiC grinding			421	
			40,865 S	
			28,931 S	
			30,651	
			2,705	
			15,791	

N.G. = Wheels did not qualify
S = Suspended - no spall

TABLE XI

Dimensional Characteristics of
Twenty Si_3N_4 Roller Blanks

Roller Number	O.D. Size	Roller Length	End Squareness End 1	End Squareness End 2	Corner Rad. End 1	Runout End 2
1	0.35598	0.35590	0.00030	0.00020	0.00050	0.00035
2	0.35597	0.35580	0.00019	0.00030	0.00030	0.00045
3	0.35606	0.35591	0.00025	*0.00030	0.00035	0.00050
4	0.35595	0.35574	0.00019	0.00020	0.00030	0.00030
5	0.35586	0.35581	0.00032	*0.00012	0.00040	0.00030
6	0.35592	*0.35571	0.00020	0.00027	0.00045	0.00035
7	0.35594	0.35592	*0.00013	0.00020	0.00030	0.00040
8	0.35596	0.35586	0.00017	0.00022	0.00040	*0.00020
9	0.35603	0.35620	*0.00050	0.00017	0.00070	0.00090
10	0.35598	*0.35628	0.00020	0.00015	*0.00110	*0.00120
11	0.35588	0.35575	0.00026	0.00022	0.00060	0.00045
12	0.35596	0.35584	0.00017	0.00020	0.00025	0.00035
13	0.35602	0.35608	0.00026	0.00018	0.00110	0.00100
14	*0.35607	0.35596	0.00015	0.00017	0.00040	0.00040
15	0.35592	0.35574	0.00025	0.00015	*0.00030	0.00035
16	*0.35583	0.35577	0.00025	0.00023	0.00025	0.00035
17	0.35598	0.35612	0.00022	0.00023	0.00080	0.00100
18	0.35596	0.35594	0.00018	0.00012	0.00090	0.00070
19	0.35590	0.35594	0.00027	0.00013	0.00045	0.00035
20	0.35599	0.35628	0.00014	0.00021	0.00080	0.00070

NOTE * - Denotes maximum or minimum value.

(3) final OD grinding, including the crown. Silicon carbide grinding wheels on a Royal Master Plunge grinder were used for step one. Two types of wheel bonds were tried. A softer wheel produced only seventeen rollers per two inch diameter of wheel removed. A harder bond produced thirty three rollers for the same amount of wheel material used. The geometry of the roller corner radii was good and well within the print limits.

End grinding and honing are done on a double disc Gardner grinder where both ends are ground at the same time. The planned procedure had been to use silicon carbide wheels throughout. Honing with aluminum oxide wheels was inadvertently attempted first however, but stock could not be removed. The operation was then transferred to the end grinder where aluminum oxide wheels were again used. On the second pass through with thirty rollers in the magazine, cracks were observed on the ends which progressed to the roller OD. Examination of the rollers that had been through the honer and one pass on the end grinder showed that two thirds of those also had cracks. Of the rollers processed through the corner radius grinder, only one third did not have detectable cracks. Of the 32 roller blanks not ground, 27 were considered good, 4 showed pinpoint defects and one showed a crack. The number of rollers left without defects were below the number needed for proper size groupings to make the three bearings.

It is felt that the rollers fractured due to the very high compressive loading which resulted when the rigidly mounted opposing aluminum oxide wheels did not remove any stock.

(c) Bearing Roller Billet Testing - Rolling contact fatigue rods were taken from the same billets as used for the bearing roller blanks. The test results are shown in Table XII. Note that the rod identification is a simple number indicating finish grinding by procedure #2 which omitted the 320 grit finish diamond grinding prior to the final lapping operation.

The initial testing at 800,000 psi Hertz stress on rods #7 and #8 (from the same billet) produced reasonable values. Further testing at lower Hertz loadings produced erratically low results, in this case regrinding with silicon carbide produced further deterioration. Rods #15 and #16 from the second billet gave initially poor results with no improvement upon silicon carbide regrinding. An intensive investigation into the causes of these poor and erratic results was then undertaken as described in the following section.

TABLE XII

Rolling Contact Fatigue Life of HS-110A Si_3N_4
Bearing roller billets

Rod Identification	Density gm/cc	Flexural Strength psi	Load lbs.	Calc Hertz Stress psi	Life 1000 Cycles
7	3.17	125,700	325	800,000	16,446
			325	800,000	33,911
			220	700,000	5,530
			100	540,000	37,446 S
			150	610,000	43,430 S
			220	700,000	7,240
8	3.17	125,700	325	800,000	28,363
			325	800,000	28,997
			325	800,000	2,921(1)
			325	800,000	1,559
			325	800,000	5,530
			220	700,000	628
			220	700,000	1,010
			220	700,000	1,270
			150	610,000	50,674 S
8 Reground with Silicon Carbide			325	800,000	196
			325	800,000	152
			220	700,000	1,908
			220	700,000	426
			150	610,000	26,368 S
11 Billet not used for rollers	3.14	123,200	325	800,000	259
			325	800,000	83
12 Billet not used for rollers	3.14	123,200	325	800,000	136
			325	800,000	70
13 Billet not used for rollers	3.16	118,300	325	800,000	223
			325	800,000	86
			325	800,000	724
			220	700,000	1,347
			100	540,000	267
			100	540,000	44,978
14 Billet not used for rollers	3.16	118,300	325	800,000	328
			325	800,000	375
			220	700,000	590
			100	540,000	16,886
			220	700,000	300
			150	610,000	3,146

TABLE XII
continued

Rod Identification	Density gm/cc	Flexural Strength psi	Load lbs.	Calc Hertz Stress psi	Life 1000 Cycles
15	3.17	124,900	325	800,000	[illegible]
			325	800,000	1,201
			325	800,000	3,871
			325	800,000	63
			220	700,000	206
			220	700,000	84
			150	610,000	53,648 S
			150	610,000	3,082
16	3.17	124,900	325	800,000	836
			325	800,000	40
			325	800,000	636
			100	540,000	24,109
			150	610,000	1,189
			100	540,000	15,028
			150	610,000	28,610 S
16 Reground with Silicon Carbide			325	800,000	122
			325	800,000	82
			220	700,000	64
			220	700,000	230
			150	610,000	750
			150	610,000	752

(1) Failed through surface defect
S Denotes suspended test

D. ANALYSIS OF ROLLING CONTACT FATIGUE TEST RESULTS

1. Introduction

This section will deal with the examination of the RCF rods after fatigue testing. Chronologically, the RCF rods fell into two groups. The first group is identified by the letters FM preceding a number. The second group is designated by a straight number. Taken as groups, the first group performed relatively well and the second poorly in the fatigue tests. The prime objective of the examination was to determine the cause(s) of the difference in performance between the two sets of rods. It has been found convenient and natural to reference the two groups as the first and second throughout this section.

The examination consisted of scanning electron microscopy (SEM) of the rod surfaces, electron beam probing, bulk density determinations of individual rods, light and scanning electron microscopy of polished cross-sections. The experimental observations are followed by a discussion and the section ends with a summary and conclusions.

Table XIII presents various pieces of information concerning the rods in this section. Included are finishing data, density values and strength values.

2. Experimental Observations

a. Surface Characterization of the RCF rods with the Scanning Electron Microscope (SEM).

The external surfaces of eleven of the rods used in the fatigue experiments were examined in a combination instrument containing an SEM and an electron probe. The surfaces were viewed at magnifications ranging from 50 to 5000 times with 500X being a good magnification for general comparative purposes. (When magnifications are mentioned, the horizontal magnification of the SEM photographs is being referenced.)

i. Examination of Unloaded Surfaces - As may be seen from Table XIII, various rods received four distinctive final finishing operations. The operations and corresponding photographs of representative areas are listed below. For two of the four finishes a second photograph was included to show typical details not evident in the first.

(1) Rough grinding with a 100 grit diamond wheel followed by final finishing with a 320 grit diamond wheel. The circumferential grinding scratches are readily visible as seen in Figure 16.

(2) Preliminary finishing the same as (1) above with additional finishing done by means of a leather lap impregnated with diamond dust while the rod rotated in a chuck. The

TABLE XIII

Summary of Selected Information on the RCF Rods

Identity	Billet Density (g/cc)	Rod Density (g/cc) Water Displacement Method	Rod Density (g/cc) Pycnometer Method	Billet Strength (psi)	Finishing History
FM-1	N.A.	3.21	3.20	N.A.	Rough grind with 100 grit diamond wheel, followed by grinding with a 320 grit diamond wheel
FM-3	3.18	3.19	-	122,700	As for FM-1 plus lapping with diamond impregnated leather strap
FM-4	3.15	3.16	-	N.A.	" " "
FM-10	3.11	3.19	3.18	112,400	" " "
FM-11	3.19	3.18	-	130,900	" " "
FM-7	3.20	3.19	-	138,600	As for FM-3, initially; then lightly reground with a SiC wheel
9	3.18	3.17	-	137,400	Rough grind with a 100 grit diamond wheel, followed by machine lapping with fine diamond grit
12	3.14	3.10	3.09	123,200	" " " "
13	3.16	3.16	-	118,300	" " " "
15	3.17	3.17	-	115,800	" " " "
8	3.17	3.18	-	117,200	As for #9, initially; then lightly reground with a SiC wheel

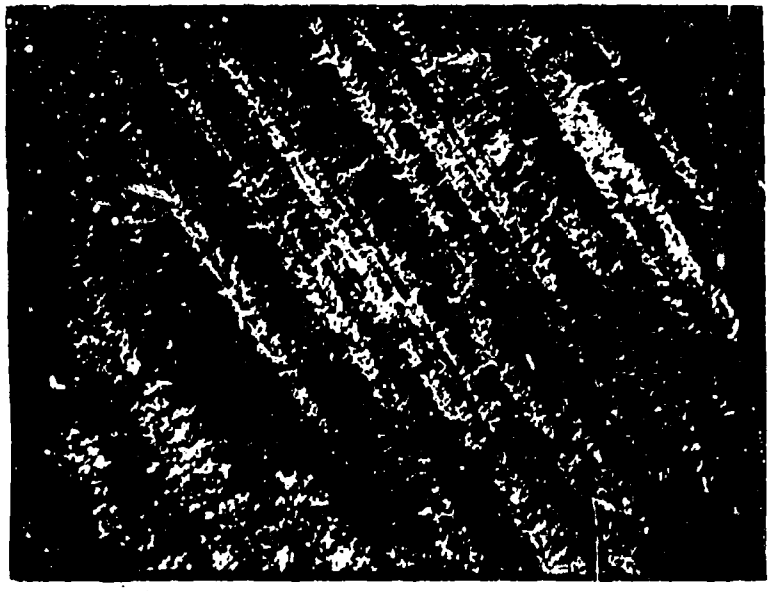

FIGURE 16 Surface as finished with a 320 grit diamond wheel. Rod FM-1. 500X SEM

purpose of the lapping was to reduce the rms surface roughness. As may be seen in Figures 17 and 18, this goal was achieved by removing to a greater or lesser extent the 320 grit scratches.

(3) Regrinding with a silicon carbide wheel. This finishing, present at the time of the SEM investigation, was done after the rods were initially fatigue tested in their original finish. Two of the rods examined possessed this finish; FM-7 which was originally finished as in (2) above and #8 which was originally finished as in (4) below. The regrind consisted of removing less than 0.001 inch from the rod. Figure 19 shows the appearance of this finish.

(4) The rods were rough ground to cylindrical shape with a 100 grit diamond wheel and taken to final finish by a machine lapping procedure using 4-8 micron diamond paste. Figures 20 and 21 portray the appearance of this finish. Occational, fine, non-circumferential scratches, that were produced by the machine lapping method, are visible in Figure 21.

The above mentioned photographs were taken from areas on the rods which were not in contact with the load-applying wheels of

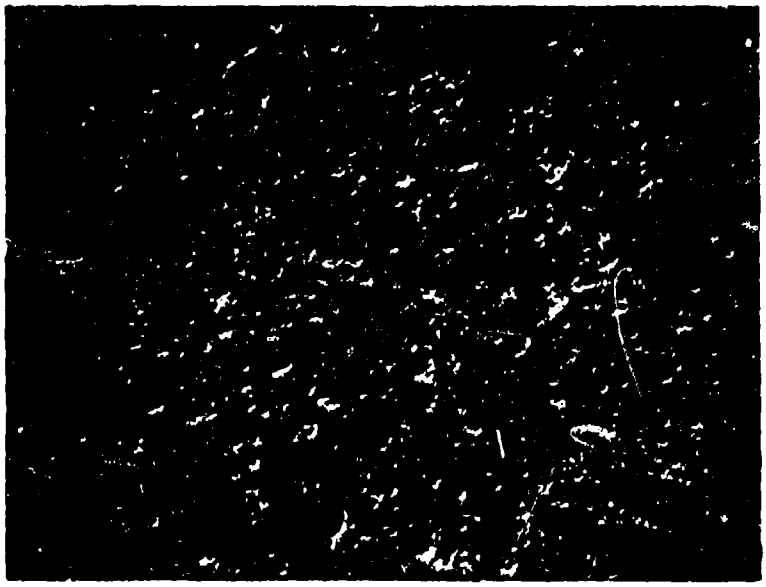

FIGURE 17 Surface as finished with impregnated leather lap on the 320 grit ground surface. Rod FM-3 500X SEM

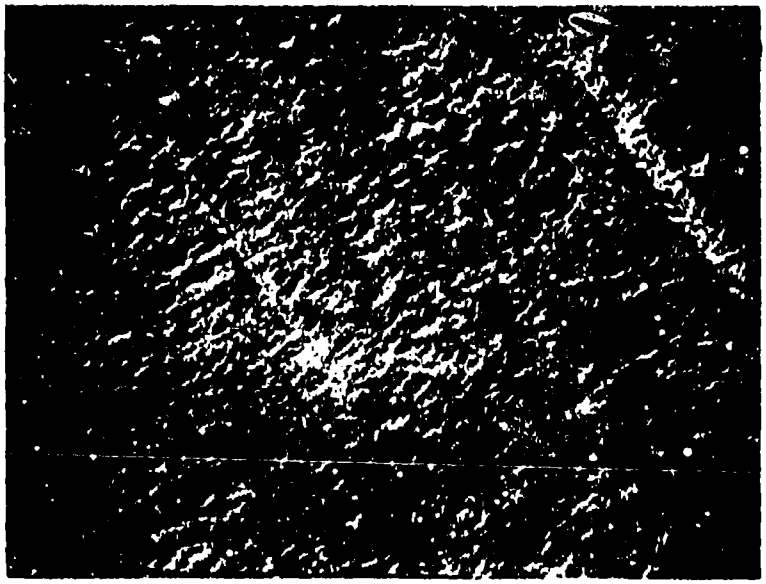

FIGURE 18 Surface as finished with impregnated leather lap showing residual grinding scratches. Rod FM-4 500X SEM

FIGURE 19 Surface as reground lightly with a silicon carbide wheel. Rod FM-7 500X SEM

FIGURE 20 Surface as finished by machine lapping after grinding with a 100 grit wheel. White features are artifacts of silver paint. Rod #12 500X SEM

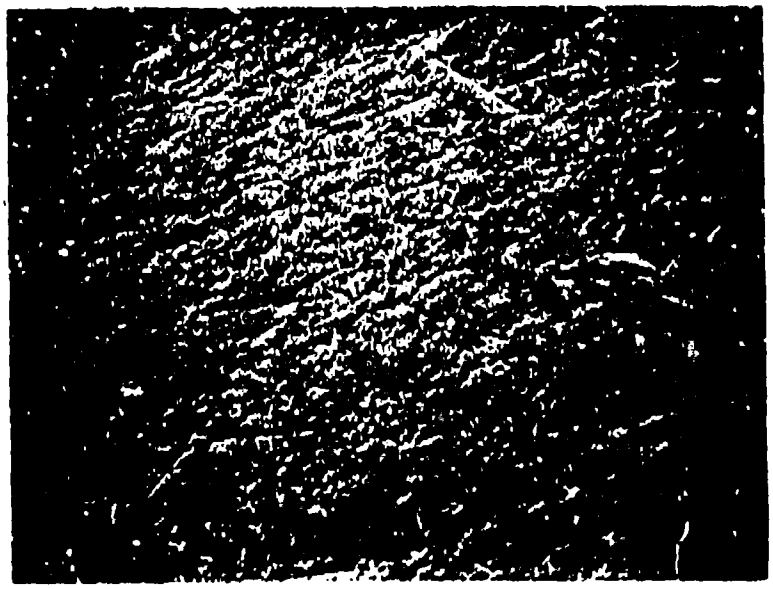

FIGURE 21 Surface as finished by machine lapping showing random lapping scratches. Rod #15 500X SEM

the fatigue test machine. Therefore they represent the condition of the surfaces prior to fatigue testing. The four separate finishing methods give rise to distinctive surface appearances. If the differences from the frequency and orientation of grinding and lapping scratches are neglected, the appearance of the leather lapped and the machine lapped surfaces are quite similar. An important exception to this general statement concerns rod #12. Figure 22 shows an area from this rod which contains relatively larger and deeper pits than were observed on other rods.

ii. Examination of Spalls - The formation of a spall in the load track leads to automatic termination of a given RCF test run. Examples of spalls are shown in Figures 23 through 28. There appears to be three modes of spall formation: initiation by inclusions, initiation by sideways branching of a circumferential crack and initiation from surface pits.

The first mode is shown in Figure 24. The dimpled region just below the center of the photograph was found to possess an inclusion rich in Mg and Al as determined by the electron probe. It is maintained that the crack of the spall was initiated at the inclusion as a result of a stress concentration there. Inclusions of similar composition have been found in other studies of HS-110 silicon nitride material. The apparent point of fracture initiation of the spall surfaces were often examined with the electron

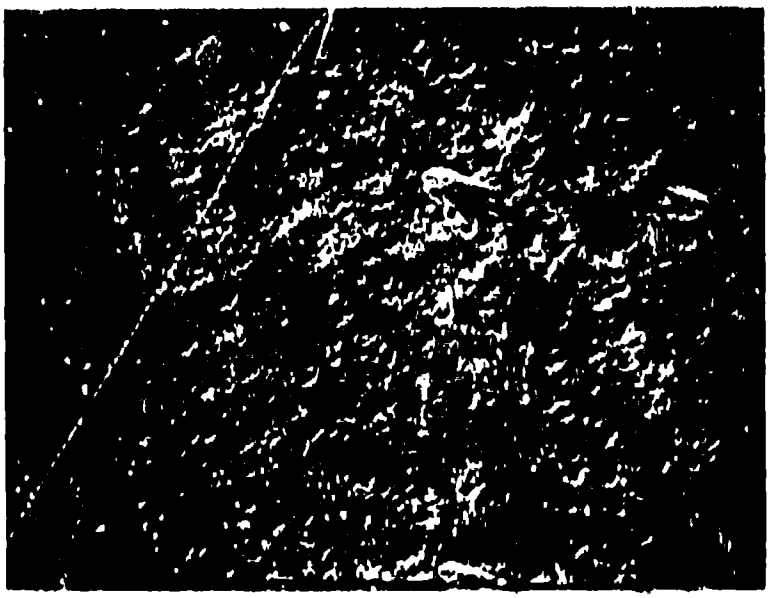

FIGURE 22 Relatively large and deep surface pits on, and unique to, Rod #12. 500X SEM

FIGURE 23 Wear spall on Rod FM-1 75X SEM

FIGURE 24 Wear spall on rod FM-3. 200X SEM
Failure believed to have been initiated from inclusion just below center.

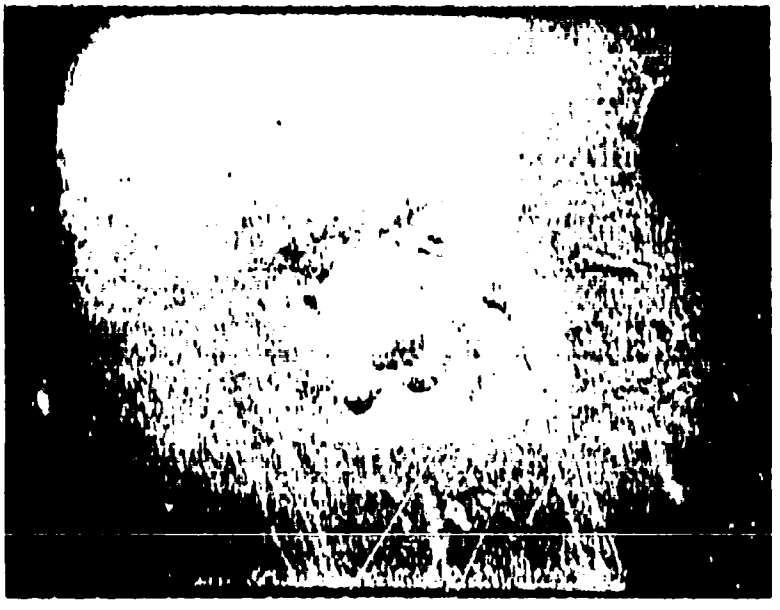

FIGURE 25 Wear spall on rod FM-11. 500X SEM
Note presence of cracks at boundary of loaded track.

probe in an effort to detect evidence for the presence of inclusions. In the majority of the cases an actual inclusion was not found. This is not an unexpected result, even if an inclusion had been initially present and was the cause of spalling, because material is lost upon spalling and because the rod remains in contact with the loading wheels for a few revolutions after spall formation. Occasionally, a region of a spall was found to possess a diffuse higher concentration of known impurity elements which were not localized at an inclusion. In those cases where an inclusion was found, it was not always possible to ascertain whether the inclusion nucleated the spall or whether it was simply uncovered by the propagation of the crack of the spall.

The second mode of spall formation is shown in Figure 26. It is believed that circumferential crack, which intersects the rods surface at the boundary of the loaded track, has branched underneath the loaded surface, eventually producing the spall. The nature of boundary cracks is more apparent in Figure 25, where they are seen to parallel the load track. Boundary cracking occurs frequently but is not always responsible for a spall. Boundary cracks may adjoin only one or both sides of the loaded track and sometimes circle the rod for a substantial fraction of the circumference. Figure 29, which is a higher magnification of the RHS of the spall in Figure 25, shows that the boundary cracks are often layered and inclined at an acute angle to the cylindrical surface.

The relative importance of this second mode of spall formation can not be fully evaluated. During the course of the fatigue experiments, some trials were terminated and the results not used because of either known improper experimental test conditions or the failure of the loading wheels to qualify. Insomuch as non-uniform loading could be expected to promote boundary cracking, some of the spalls examined and shown could have been formed from discarded test runs. Unfortunately, a given load track could not always be correlated with its history of formation at the time the rod was subsequently examined.

The third proposed mode of spall formation involves the enlargement of surface pits to an extent sufficient to nucleate a spall crack. Figure 30, which is an enlargement of the feature seen just above center in Figure 27, shows what is believed to be an embryonic spall of the third mechanism. The termination of the RCF trial by the formation of the spall at the bottom of Figure 27, is believed to have aborted its growth. The area surrounding the void and the walls of the void, as far in as was possible to reach, were extensively probed to find evidence of an inclusion without success.

Figure 31 shows a portion of the wall of a spall, the central feature of which could be either a surface pit or pore. The fact that test lubricant can be seen oozing from the recess, even after prolonged rod cleaning in an ultrasonically agitated acetone bath,

FIGURE 26 Wear spall on Rod #8. 100X SEM
Failure believed to have been initiated
from boundary crack.

FIGURE 27 Wear spall on rod #12. 50X SEM
Note pit enlargement in loaded track.

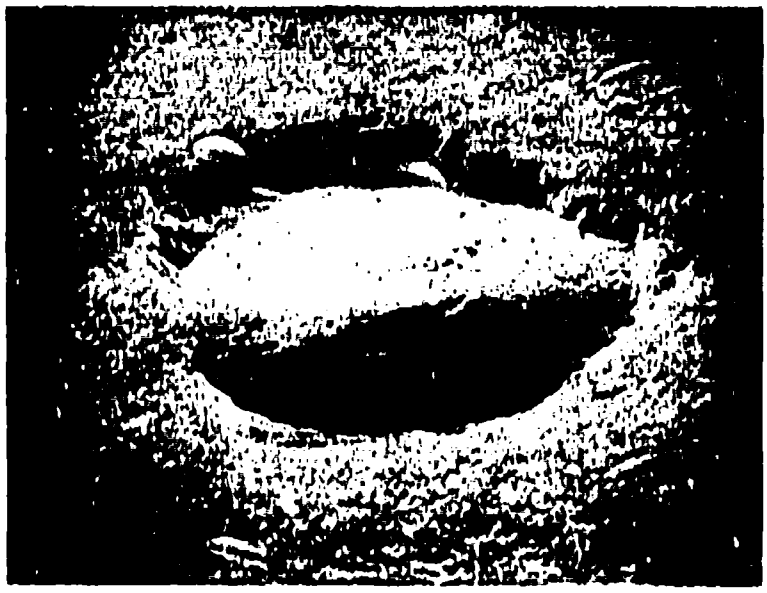

FIGURE 28 Wear spall on Rod #13. 150X SEM
Note presence of large pits in the load track.

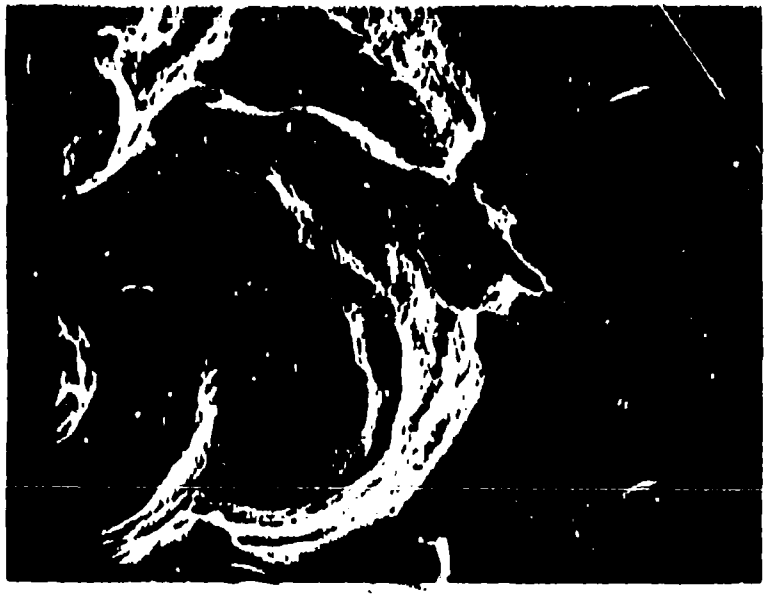

FIGURE 29 Higher magnification of RHS portion of spall in Figure 25 showing structure of boundary cracks. 200X SEM

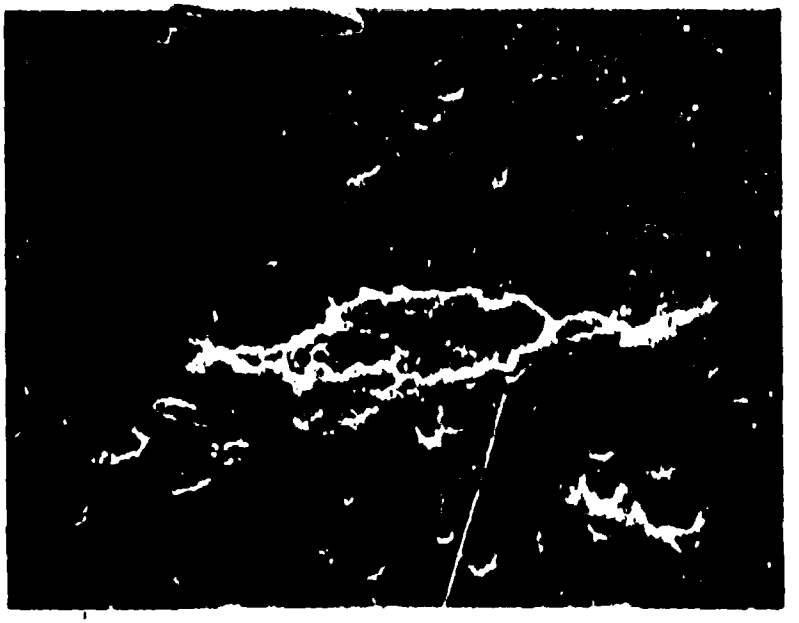

FIGURE 30 Enlargement of pit above center in Figure 27, believed to be incipient spall. 500X SEM

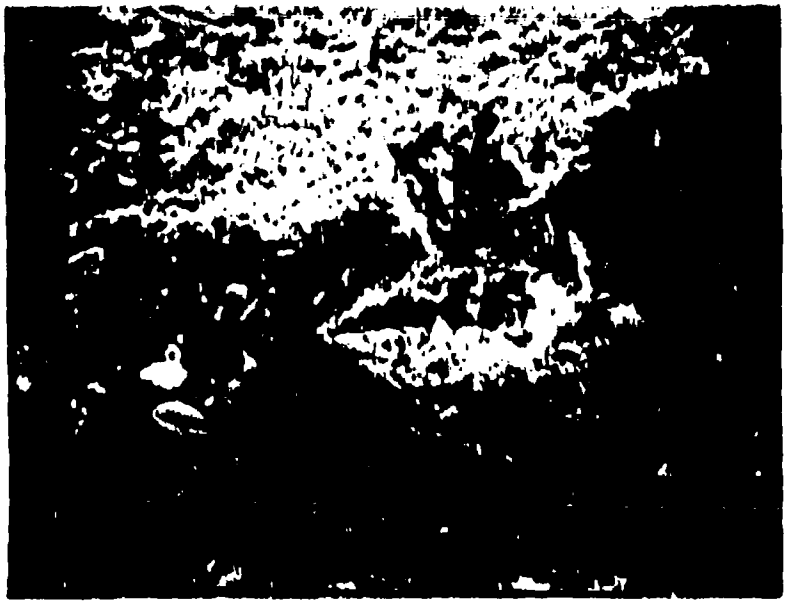

FIGURE 31 Possible exposed pore or surface pit on wall of spall. Residual lubricant visible Rod #15. 1000X SEM

indicates that the feature was probably in existence during the fatigue test. While this location could conceivably have been the initiation point for the spall, no fractographic evidence is available to support (or refute) this possibility.

Aside from the evidence presented so far, direct evidence for this third mechanism is meager from the examination that has been preformed on the spalls themselves. Additional evidence for this mechanism will be presented in the next sub-section and the matter will be renewed in the discussion section.

iii. Examination of Load Tracks - The appearance of wear tracks of rods having the four classes of finishing operations are shown in Figures 32 through 35. A comparison of these photographs with the corresponding photographs (Figures 16 through 21) of rods having a particular finish shows the surface alterations as a result of the fatigue testing.

Figure 32 shows the worn track of the rod whose final finish was produced with a 320 grit wheel. As a result of the wear, the grinding scratches are shorter and their finite length is now apparent at this magnification. Some fine scale wear has produced a pattern of small elongated pits whose major axis is perpendicular to the direction of rod rotation (and to the axis of the grinding scratches). This latter structure can be seen more clearly at the higher magnification of Figure 36. In addition to the pits, a fine series of steps, perpendicular to the rolling direction, is also evident. A comparison of Figure 36 with Figure 37 of an unloaded region at the same magnification suggests that the growth of the elongated pits may have been assisted by the removal of strongly disturbed material between adjacent grinding scratches.

The wear track of a rod finished with the leather lap, shown in Figure 33, again indicates minute wear by the almost complete disappearance of any traces of grinding scratches. A comparison of loaded areas (Figures 33 and 38) with unloaded areas (Figures 17 and 18) shows that little, if any, growth of the pits has occured as a result of fatigue testing.

The wear track of a rod which had been reground with a silicon carbide wheel is shown in Figure 34. Although the regrind produced the finish with the smoothest areas, the smooth areas are seen to consist of a burnished layer which is partially removed by the application of a load. The removal of the surface skin implies an alteration of the surface properties during regrinding. However, this treatment did not significantly affect the performance of the so finished rods, which had been previously tested with their original finishes.

A very distinctive feature of wear tracks on the rods of the second group are large pits. An example is shown in Figure 35. Although this area is from the same rod (#12) that had large pits on its unloaded surfaces, the size of the load track pits are

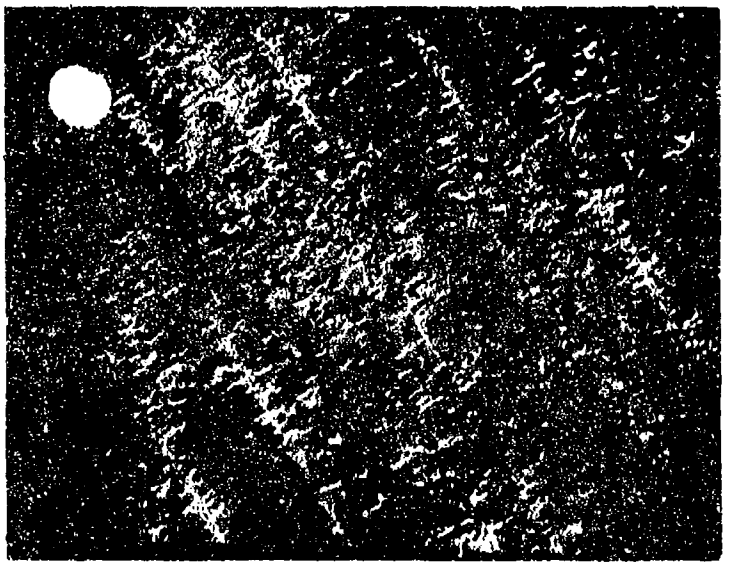

FIGURE 32 Appearance after fatigue testing of 325 grit ground surface. Rod FM-1 500X SEM

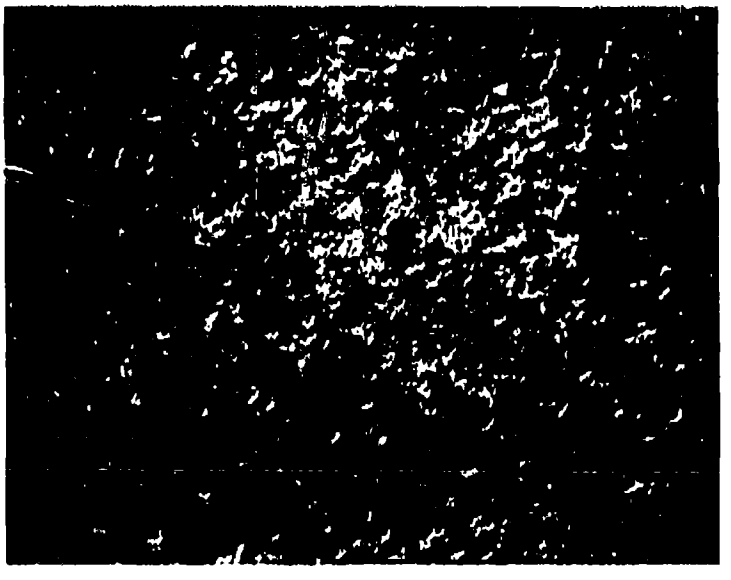

FIGURE 33 Appearance after fatigue testing of leather lapped surface. Rod FM-3 500X SEM

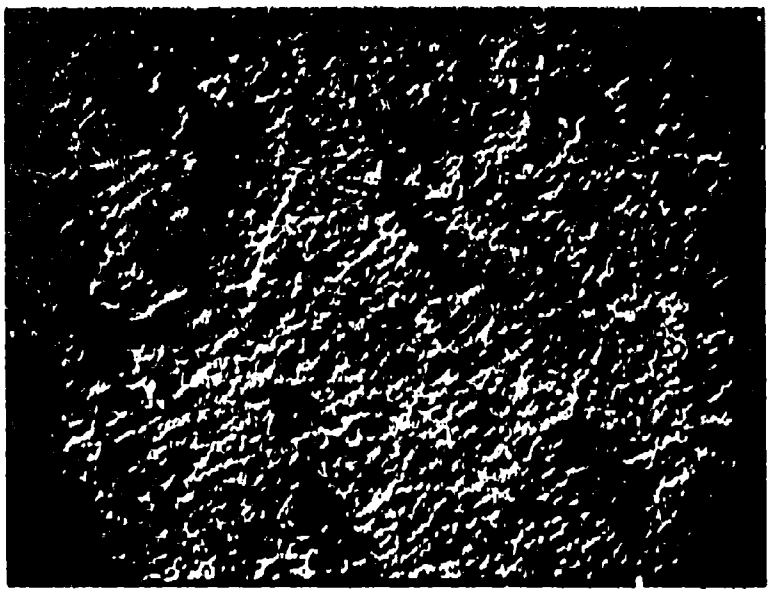

FIGURE 34 Appearance after fatigue testing of surface reground with SiC wheel. Rod PM-7 500X SEM

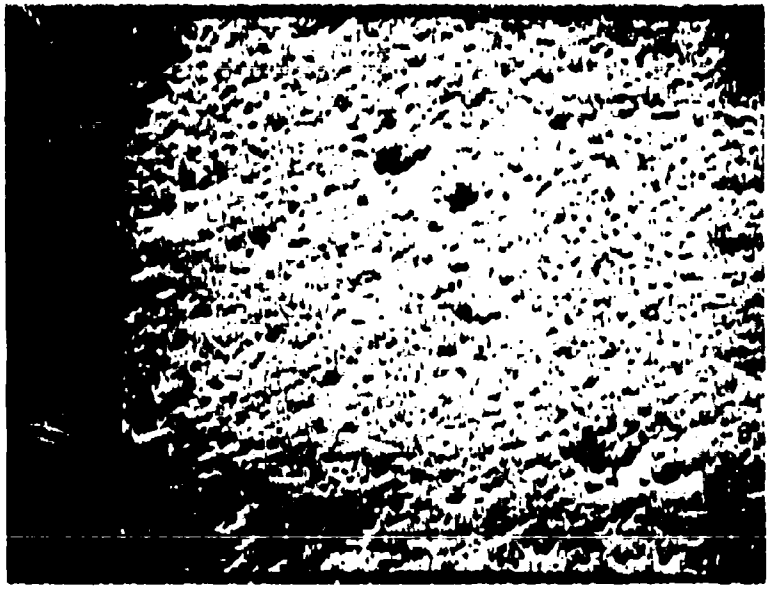

FIGURE 35 Appearance after fatigue testing of surface machine lapped after 10C grit grind. Rod #12 500X SEM

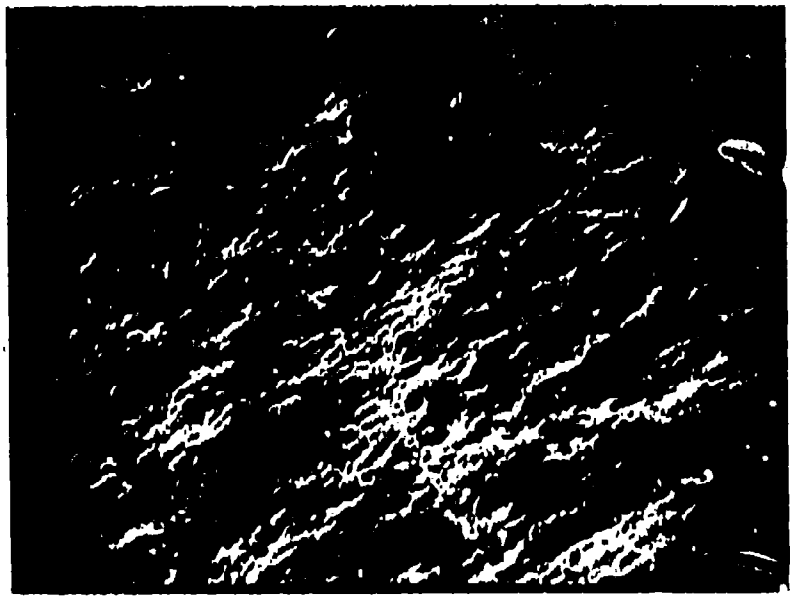

FIGURE 36 Higher magnification of worn 325 grit ground surface showing elongated pits and stepped appearance. Rod FM-1 2000X SEM

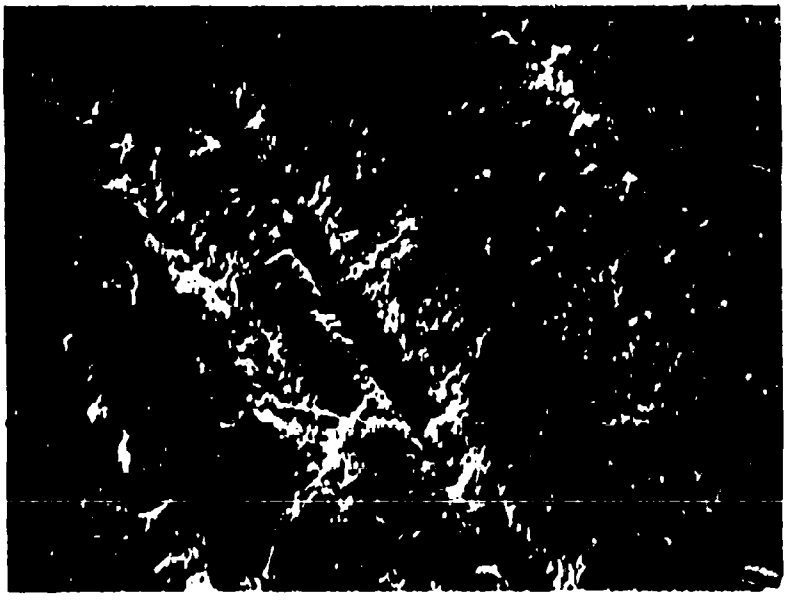

FIGURE 37 Higher magnification of surface finished with 325 grit wheel. Rod FM 1 2000X SEM

FIGURE 38 Another example of worn track on a leather lapped surface. Rod FM-4 500X SEM

considerably larger, as a comparison of Figures 35 and 22 shows. Nor are these large pits unique to Rod #12. Other instances of large pit development may be seen in Figures 27, 39 and 40. The development of these large pits has been observed only on the second group of rods and is believed to be related to the failure mechanism of this rod group. That the pits enlarge under the action of the applied load is clearly shown in Figure 27.

b. Rod Density Determinations - The physical densities of the majority of the RCF rods was measured by a water displacement method, with corrections for water temperature. The densities are recorded in Table XII. In addition, the densities of three of the rods were remeasured by a more accurate method: pycnometry with xylene as the immersion fluid. The duplicated determinations agreed to within 0.01 g/cm^3.

Is is seen that the density of Rod #12 was very low. The average density of the billet, from which this rod was cut, was 3.14 g/cc. Unfortunately, the billet possessed a considerable density variation and the rod was excised from a low density portion of it.

c. Examination of Polished Sections - Circular cross-sections of rods #12, #8, FM-7 and FM-10 were polished for microstructural examination. As the primary purpose of the examination

FIGURE 39 Example of development of large pits in loaded track. Rod #13 150X SEM

FIGURE 40 Example of development of large pits in loaded track. Rod #15 290X SEM
Dark streaks are artifacts

was to ascertain the porosity content, the samples were not etched. Examination was by optical and scanning electron microscopy.

Figures 41 through 44 were taken by a phase interference contrast method of the four respective cross-sections. All samples were found to contain some porosity. The porosity in the photographs shows (with difficulty) as relatively large white spots, often with a black speck at the bottom of the pore as a result of the light interference. The photographs are not of representative areas, as selected areas, which contained porosity, had to be found.

Figures 45A through 48A are randomly selected views of the four sections taken in plane polarized light. Figures 45B through 48B were taken with cross-polarized light of the same corresponding areas. As a result of the ability of cross-polarized light to penetrate the surface and render visible sub-surface detail, the latter series of figures enables one to obtain an idea of the scale of the microstructure and a measure of the material's uniformity.

Due to the general inadequacy of the light microscope pictures to clearly delineate the porosity, an SEM was used for this purpose. Figure 49A of rod #12 shows the porosity as the larger white specks. The contrast is obtained largely as a result of the presence of elements of widely different atomic numbers which have different yields of secondary-electron production. The silicon nitride appears dark while locations of heavier elements appear light. Lead, from a lead lap used in the polishing operation, has collected in the pores and effectively serves to signal their location. The smaller white specks are small inclusions containing primarily either tungsten or iron. Figure 49B is an enlarged view of the pore in the upper left corner of Figure 49A.

Figures 50, 51 and 52 show porosity in the remaining three cross-sections. The impacted lead has been removed from the pores of these samples by ultrasonic cleaning. Pore contrast is achieved primarily by changes in surface contour. The pores are generally lighter at the bottom of the photographs than at the top. White specks, representing inclusions of the heavier elements, are still present.

3. Discussion

a. Introduction - The sharp change in fatigue life between the two main rod groups is an experimental fact. It is the purpose of this discussion to clarify the reasons for this observed shift. Any attempt to explain the difference in fatigue life between the two groups should do so on a group basis because the RCF results varied on a group basis. The probability that the relative success of each and every rod must be explained on the basis of its unique characteristics is low. It is more probable, simpler, and, as we shall see, possible to adequately explain the fatigue lives on a group basis.

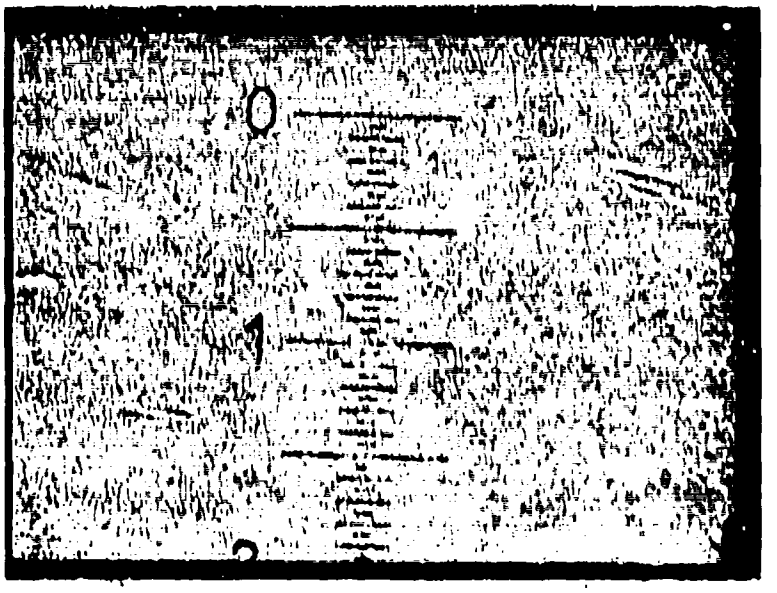

FIGURE 41 Porosity in rod #12. Phase-interference contrast microscopy 560X

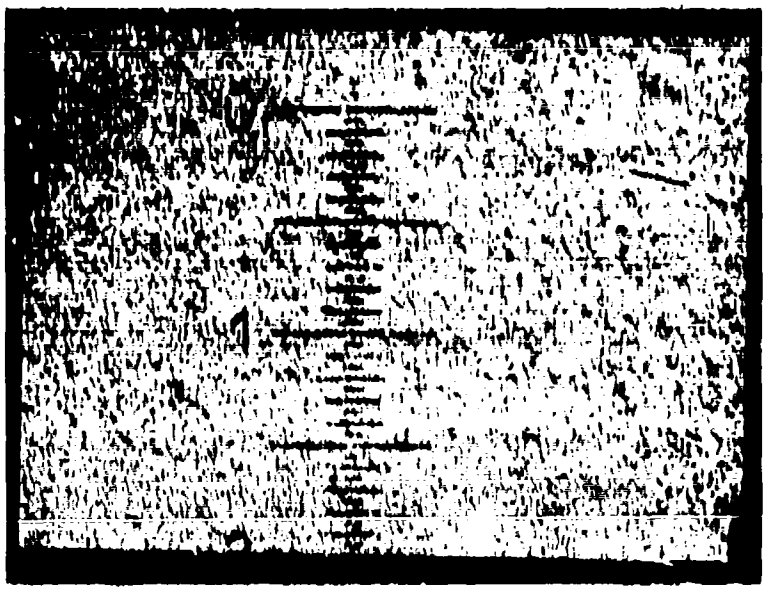

FIGURE 42 Porosity in rod #8. Phase-interference contrast microscopy. 560X

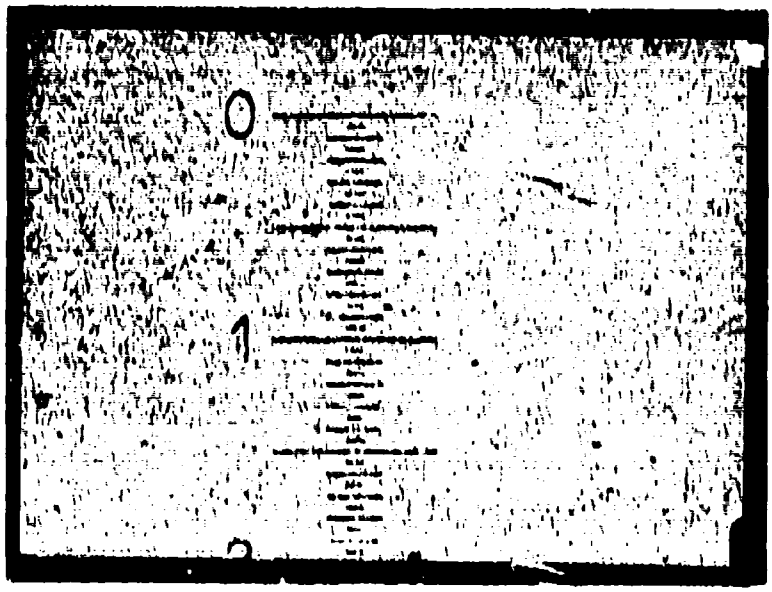

FIGURE 43 Porosity in Rod FM-7. Phase-interference contrast microscopy. 560X

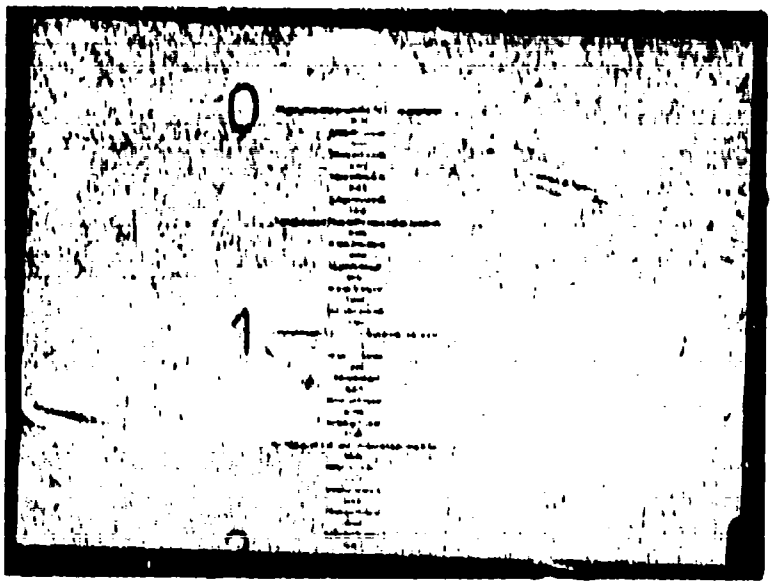

FIGURE 44 Porosity in rod FM-10. Phase-interference microscopy. 560X

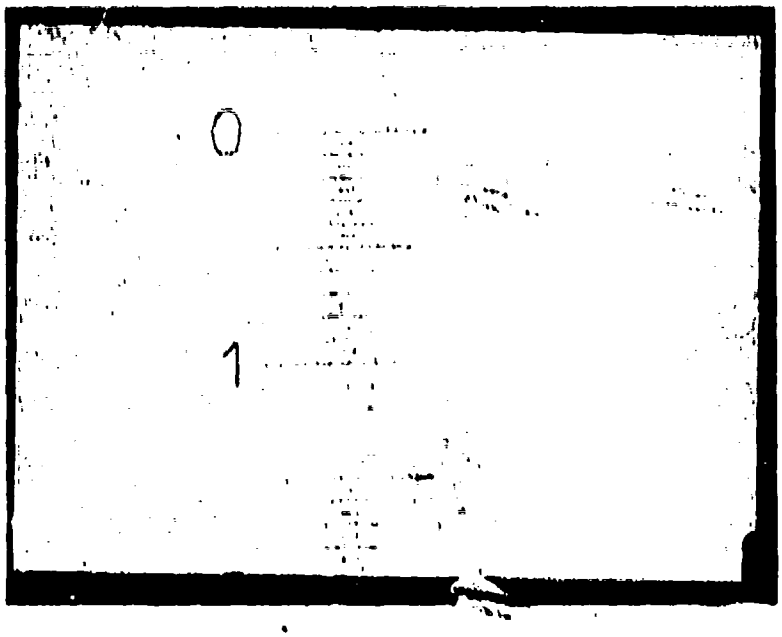

FIGURE 45A Polished surface of rod #12. Plane-polarized light. 560X

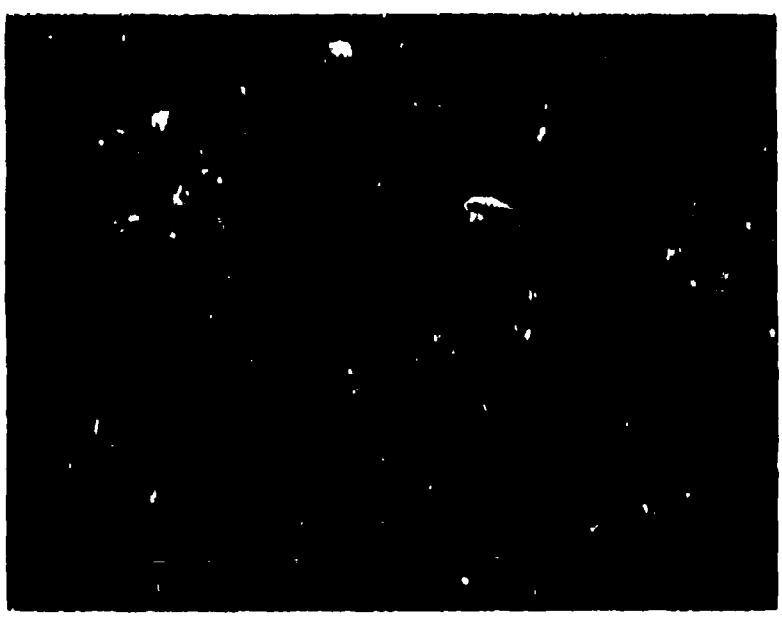

FIGURE 45B Same area as in Figure 45A. Cross-polarized light. 560X

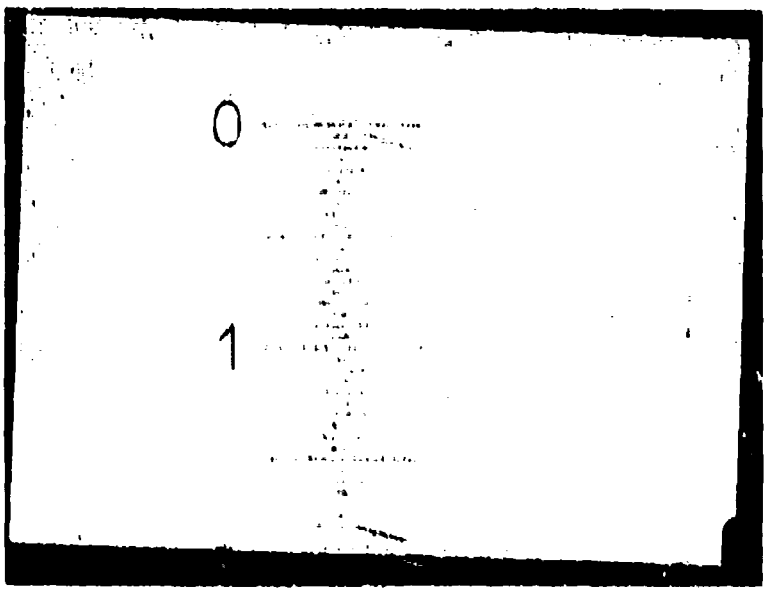

FIGURE 46A Polished surface of rod #8. Plane-polarized light. 560X

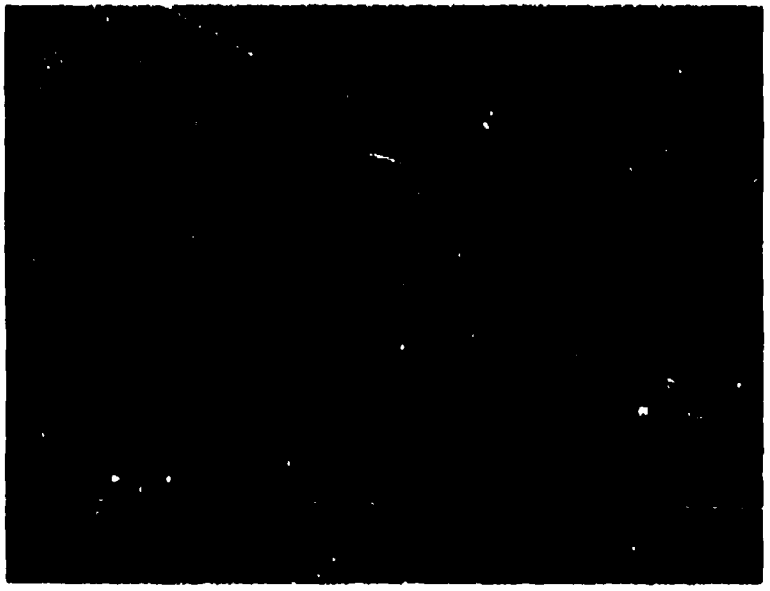

FIGURE 46B Same area as in Figure 46A. Cross-polarized light. 560X

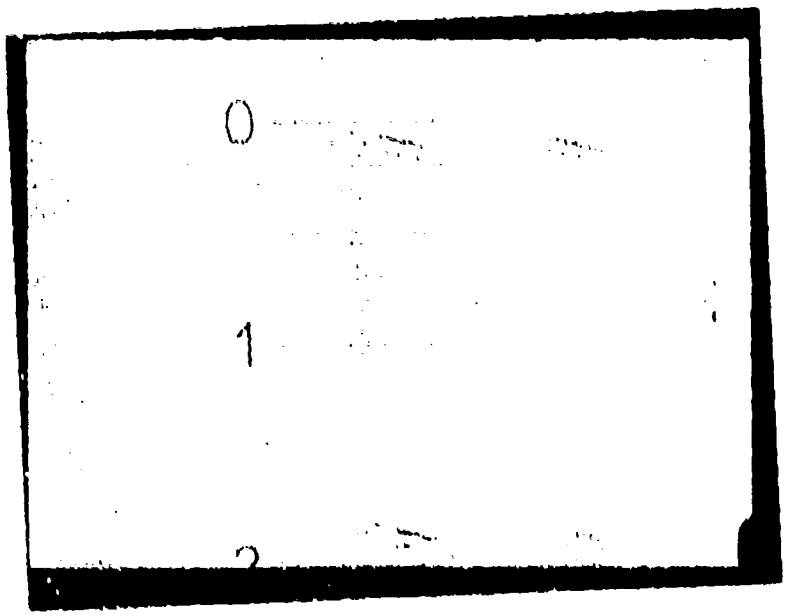

FIGURE 47A Polished surface of rod FM-7. Plane polarized light. 560X

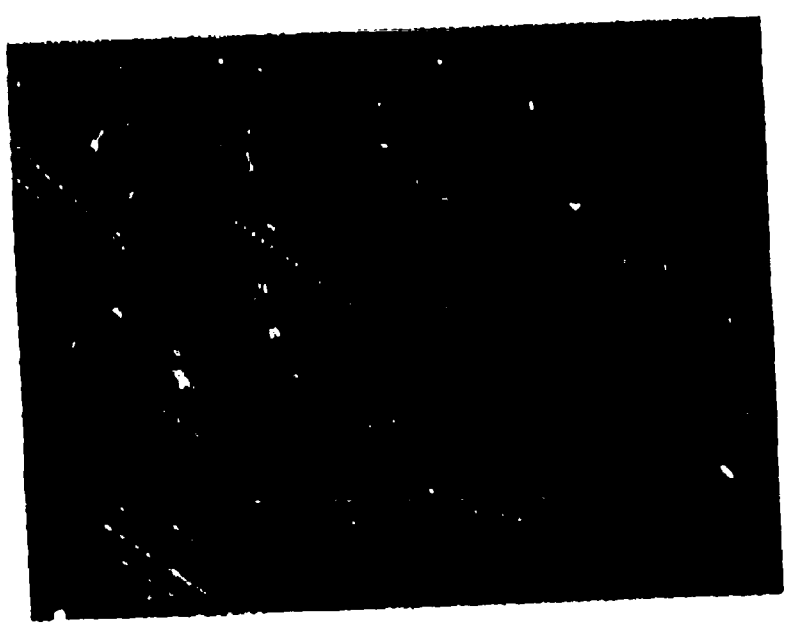

FIGURE 47B Same area as in Figure 47A. Cross polarized light. 560X

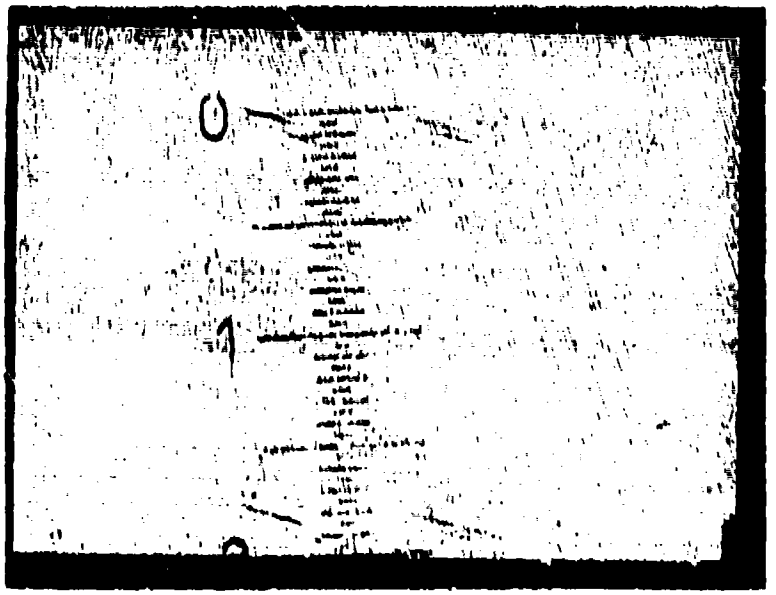

FIGURE 48A Polished surface of rod PM-10.
Plane-polarized light. 560X

FIGURE 48B Same area as in Figure 48A.
Cross-polarized light. 560X

FIGURE 49A Porosity in rod #12. 500X SEM

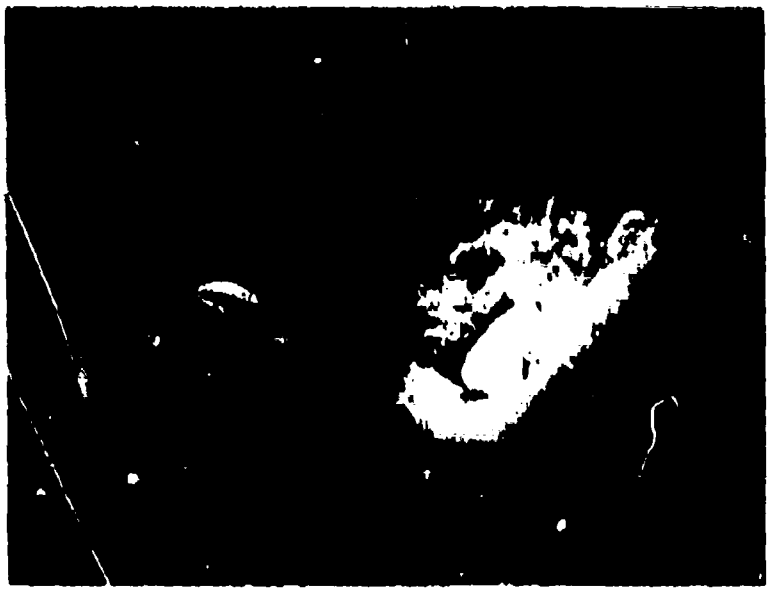

FIGURE 49B Higher magnification of pit towards lower left corner in Figure 49A. 500X SEM

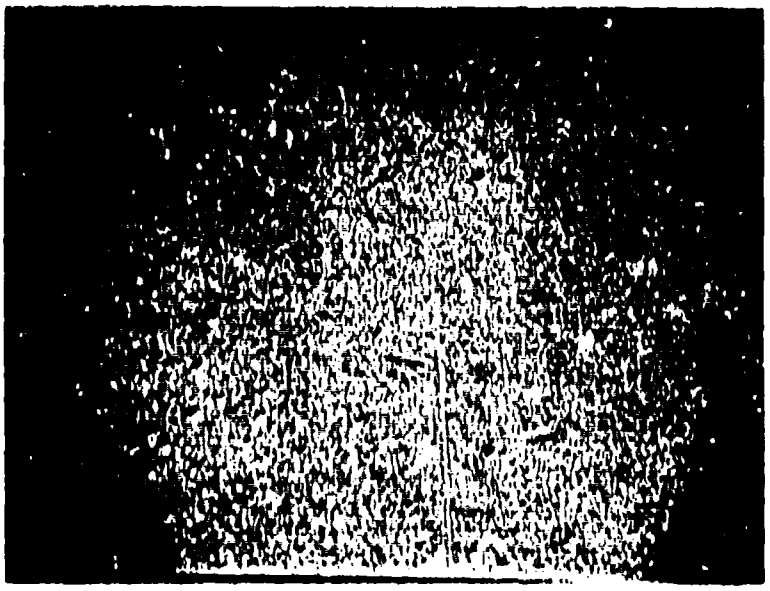

FIGURE 50 Porosity in rod #8. 500X SEM

FIGURE 51 Porosity in rod FM-7 500X SEM

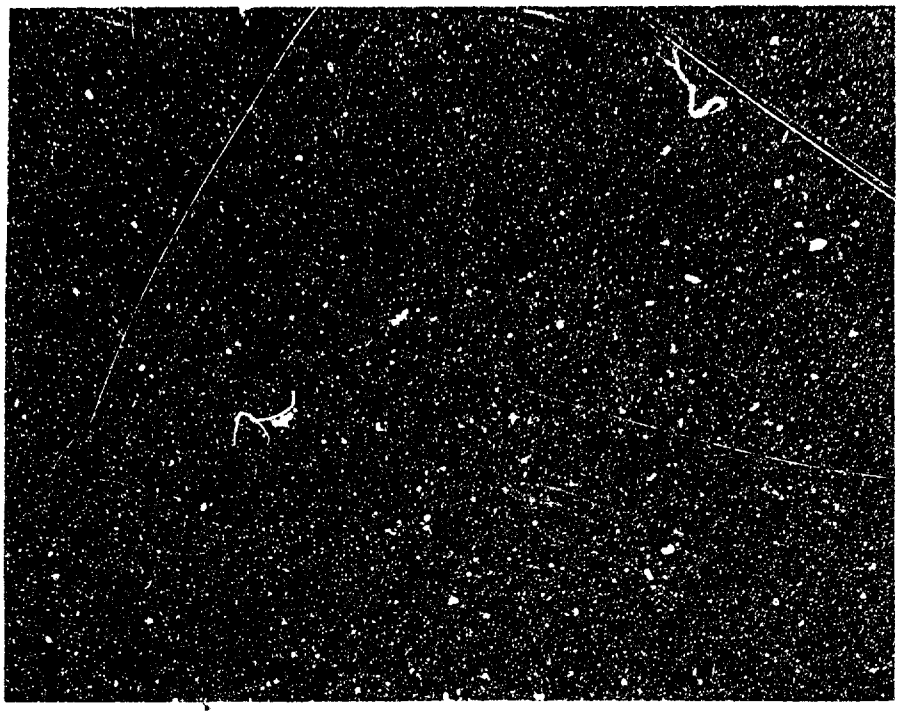

FIGURE 52 Porosity in rod FM-10 500X SEM

There are two alternatives to doing so. Either the material properties of the rods in the second group were significantly inferior or there was a consistent change in a variable unrelated to the material itself. Given that there were no significant changes in the experimental fatigue testing of the rods, the search for the material independent variable is narrowed to a processing step subsequent to billet manufacture. The central questions to be answered by this discussion are: (a) Was the behavorial shift caused by a change in the basic material or by a processing variable? and (b) What was the critical difference?

b. Lack of Evidence for a Systematic Change in Material Characteristics of the Rods - Table XIII includes a review of the bend strengths of the source billets, the billet densities and individual rod densities. A comparison of billet and corresponding rod densities leads to the conclusion that some billets (specifically, the sources of rods #12 and FM10) possessed significant density variations. It is known that some early manufactured billets had low density centers and presumeably the questionable billets are of this category.

Porosity content and tungsten concentration account for most of the variations in rod densities. An increase in one volume percent porosity decreases the density by approximately 0.03 g/cc, while a one weight percent increase in tungsten content raises the

density by roughly 0.03 g/cc. No systematic attempt has been made to explain individual rod density variations on the basis of the relative weight of the two factors. The limited examination of polished cross-sections in this study and other studies on similar material indicate that the more variable factor is tungsten content. With the exception of rod #12, the other rods in Table XII are felt to have acceptable densities.

Rod #12 was found to be consistently abnormal throughout this investigation. Its density, porosity, surface pit density and scale of microstructure are sufficiently different to mark it as a special case. Rod #11 was cut from the same billet as #12, and although not included into present study, is judged to be of similar material.

The surface integrity of two RCP rods, #11 and FM-6 was investigated by an external laboratory with the use of a krypton gas absorption technique. The technique consists of promoting the absorption and mechanical entrapment of the radioactive gas onto a surface. Surface discontinuities, such as cracks or pits, which harbor a greater gas concentration, cause greater exposures on a contacting photographic film. By means of this technique, the density of surface sites of high gas absorption was found to be approximately twice as great on rod #11 as on rod FM-6. Rods #12 and FM-4, used in the present study are sister rods to the rods #11 and FM-6, respectively. The indication of the krypton gas technique that rod #11 had a higher density of surface disruptions is in qualitative agreement with the findings of this study that (a) its sister rod possessed a higher density of pits on its as-finished surface and (b) its sister rod had an abnormally high porosity content.

One criterion used to certify the acceptability of a billet was a sampling of its bend strength. To achieve certification, the average strength in three point bending had to exceed 100,000 psi. This criterion was satisfied for all billets. However, there are some indications that the sampling statistics were inadequate for billets containing appreciable density variations. In particular, it appears that the strength values reported for the billets from which rods #12 and FM-10 were removed were not representative of the material in the rods themselves. It is well known that ceramic strength is inversely related to porosity. The very low density of rod #12 does not square with the respectable strength recorded for its mother billet. The strength is more in accord with the reported density of the billet, rather than that of the rod. On the other hand, rod FM-10 had an above average density. The reported strength for the mother billet is slightly below average and is more in accord with the overall billet density. The relative porosity content of rods #12 and FM-10 was examined by the use of polished sections and found to be consistent with the relative rod densities.

The aforementioned large billet-rod density discrepancies and the related strength variations are exceptions rather than the rule. There is no indication from the bulk of the density or strength values that the material used in the second group of rods was consistently inferior to that of the first group. The cross-polarized light micrographs of the rod microstructures also fail to show a group distinction. It is therefore concluded that the difference in group fatigue behavior is not material related.

c. Role of Surface Finishing - Attention is now focused on the methods used to finish the rods. The most striking finishing difference between the two rod groups is that in only the first group was a 320 grit diamond wheel used in an intermediate step (final step for the case of FM-1) for the production of the original finish. In the cases where the 320 grit wheel was not used, a final lapping operation followed the rough grinding with a 100 grit wheel. It is maintained that the omission of the intermediate finishing step allowed residual grinding damage to persist on the rods and that this damage directly led to early fatigue failure.

Although it is generally acknowledged that ceramic strength is strongly dependent upon surface perfection, until recently relatively few studies have been published which relate strength to surface condition for crystalline ceramics. A recommended literature source for work in this area is the proceedings of the 1970 conference held at the National Bureu of Standards.[2] Experimental work in this area has been hampered by (a) the complexity of the damage which gives rise to a difficulty in characterizing it and (b) the difficulty in obtaining reproduceable damage. The use of grinding or other multi-body abrasion processes to prepare the test surface significantly simplifies the second difficulty by producing a sufficiently high density of defects so that inter-sample variations are minimized. This advantage is partially offset by the uncertainty in the nature of the damage.

Time and budget considerations did not permit an extensive study of the RCF rod failures. However, an explanation for the change in RCF behavior between the two groups of rods may be made on the basis of the present observations, known characteristics of the material and reports from the literature. Published studies, relavant to the explanation, will now be discussed.

The surface roughness of ceramics, as measured by an instrument such as a profilimeter, does not correlate well with strength[3,4]. There are two fundamental reasons why this is true. Firstly, the large size of the stylus tip in relation to the size of many strength controlling defects precludes an accurate rendition of relevant surface features. Secondly, most roughnesses are expressed in some averaged form. From a strength viewpoint, a single surface defect, appropriately located, on a brittle material is essentially equivalent in severity to a high density of similar defects. For the above reasons, it is not surprising

that the performance of the rod with the roughest surface (rod FM-1 which was finally finished with a 320 grit wheel) was not inferior to the majority of the other rods.

A case of the insensitivity of the strength of alumina as a function of surface preparation has been observed by researchers at Southern Research Institute[4]. Of particular interest is their findings for metallographically polished, low rms finishes. The strengths of these polished samples was very similar to that of rough ground samples. A microscopic examination of the polished surfaces showed remnants of prior damage. An explanation for the insensitivity of the strength is that insufficient material had been removed in the polishing operation to reach the roots of the initial damage which continued to control strength.

The preparation of polished samples provides a relevant example. The importance of removing prior surface damage before proceeding to a successively finer scale abrasion removal process in order to obtain high quality polishes is well known to metallographers. Extra care must be taken with ceramic specimens to prevent pull-out artifacts as a result of the inability of these materials to relieve stress concentrations by plastic flow. Figure 53 shows a micrograph of a scratch on polished silicon nitride. Associated with the scratch is pitting damage initiated by the high Hertzian stresses when the scratching grit was dragged across the sample's face.

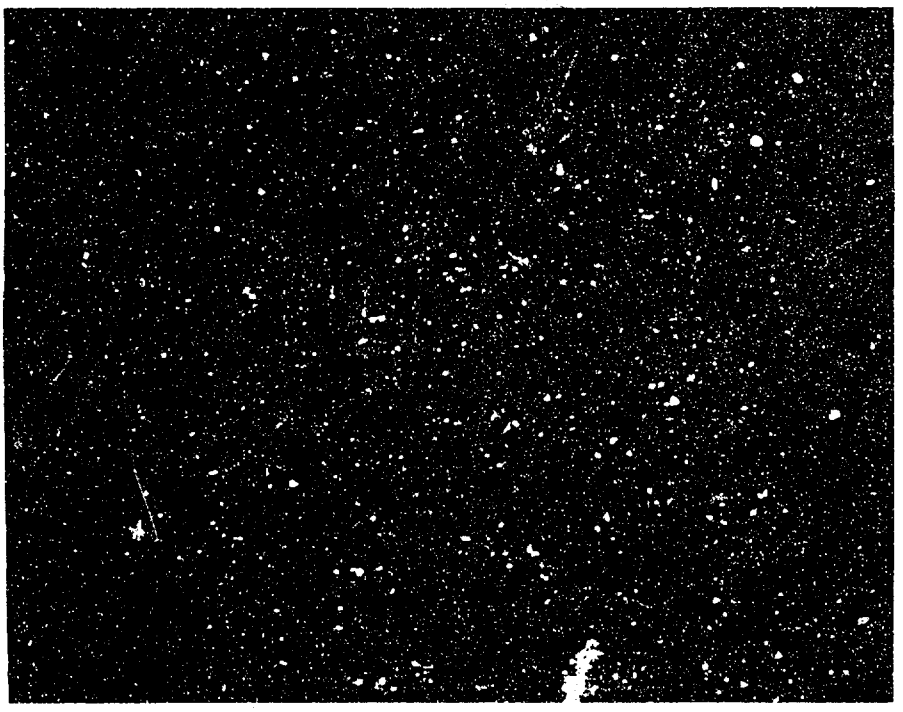

FIGURE 53 Grinding scratch with associated pitting damage on polished silicon nitride. 500X SEM

The difference in RCF behavior between the two rod groups is explained as follows. Rough grinding silicon nitride with a 100 grit wheel introduces surface damage of sufficient severity that the damage is not removed by standard lapping procedures. When the damaged surfaces are subjected to the high stresses associated with the RCF experiment, the damage sites act as pre-existing nuclei for crack formation. The result is early failure. The removal of the relatively deep 100 grit damage by subsequent 320 grit grinding removes the large nuclei necessary for surface crack formation.

Under this interpretation, the lack of a significant visual difference between the lapped surfaces that were and were not prefiously ground with a 320 grit wheel is attributed to the difficulty of spotting fine scale damage on a roughened surface. The invariant RCF results obtained before and after regrinding with a silicon carbide wheel are explained on a non-materials related basis. For the rods which performed poorly before and after the regrind, it is believed that the damage pre-existant to the regrind persisted as a result of either (a) insufficient stock removal to erase the prior damage, or (b) the further propogation of damage as a result of the rather severe grinding conditions associated with the regrind. The ability of a crack to be continuously propagated into the work during grinding has been observed in grinding sensitive steels. For those rods which performed well after regrinding, it is believed that the regrind was not sufficiently severe to introduce new damage onto a relatively undamaged surface.

The presence of relatively large pits in the wear tracks of the second group of rods and their absence from the first group is believed to reflect the differences in finishing damage between the two groups. The pits are believed to be the sites of especially severe damage. That the pits grow during loading, there is no question. The proposed main method of spall formation for the second group of rods, that is the transition from grinding damage to pit to spall, is mechanistically different from that believed to be operative in the first group. If the same mechanism, but with a different incubation time, were operative in the first group, large pits should also be observed in their wear tracks. There were none. The kinetics of spall formation for the two groups is consistent with a two mechanism interpretation, with a surface mechanism having the faster kinetics. The suggested main mechanism of spall formation for the first group of rods is crack nucleation and growth at inclusions. Although an insufficient number of spall initiation points were conclusively identified for a firm, statistically significant judgement, it is the author's opinion that more of the spalls on the longer lived rods were associated with inclusions than were the spalls on the shorter lived rods.

It has been remarked that rod #12 was atypical as a result of its large porosity content. The unique, large pits that were present on the as finished surface of this rod are probably

exposed porosity. The pores themselves are expected to act as sources for cracks during loading. In such an event, the RCF performance would be independent of surface finish processing.

4. Summary and Conclusions

An investigation was undertaken to clarify the cause(s) of variations experienced in the fatigue life of the RCF rods. The investigation consisted of (a) surface characterization of the RCF rods by means of a scanning electron microscope-electron probe combination instrument, (b) a determination of individual rod densities and (c) an examination of polished cross-sections of selected rods by light and scanning electron microscopy.

The information yielded by this study was combined with other known information on the silicon nitride material to reach the following main conclusions.

(1) The discrepancy in fatigue life between the two chronologically separable rod groupings is believed to be traceable to a change in rod finishing procedures.

(2) The critical difference in finishing procedure is believed to be the use or omission of an intermediate grinding operation with a 320 grit diamond wheel subsequent to rough grinding with a 100 grit wheel. Failure to include the 320 grit grind leaves residual rod surface damage which then controls fatigue life by acting as nuclei for crack formation.

(3) The reduced fatigue lives could not be explained on the basis of a consistent degradation in material characteristics.

(4) Excessive material porosity can result in shortened RCF life, as was found for an anomolus rod.

(5) Insomuch as the prime failure mechanism in sufficiently dense and properly finished silicon nitride RCF rods is believed to be inclusion initiated spalling, an increased fatigue life may reasonably be expected from rods made with a silicon nitride material that is more free of inclusions.

E. REPLACEMENT BEARING ROLLERS

The roller grinding problem caused the testing of the full roller bearing to be postponed. However, preparation to test bearings is proceeding utilizing the knowledge gained in surface studies and full bearing tests are scheduled during the next reporting period.

A new group of RCF test rods have been finished by procedures which include a 320 grit diamond wheel grind prior to final lapping. Very preliminary RCF tests results (falling in the next

reporting period) indicate performance in the range of the original screening results.

It is planned to proceed with fabrication of new rollers by similar stepwise diamond grinding procedures with only the final crowning operation performed by SiC grinding.

V. CONCLUSIONS AND RECOMMENDATIONS

A. Conclusions

High strength fully dense silicon nitride appears to be the most promising ceramic for evaluation in heavily loaded rolling contact bearing. Under certain conditions in rolling contact fatigue testing lives approximately three times those for CVM M-50 are obtained. However, performance in an actual roller bearing has yet to be determined.

Silicon nitride appears to be a unique ceramic in that it fails by spalling in a manner very similar to bearing steel failures rather than by catastrophic cracking.

The surface condition of silicon nitride appears critical to rolling contact fatigue life. Surface preparation should include a 320 grit diamond grinding operation to remove any sub-surface damage done by coarser grit wheels prior to any final lapping operation.

Porosity and inclusions provide points of crack nucleation and their reduction in silicon nitride should result in increased performance.

B. Recommendations

1. Full bearings be fabricated and run as originally planned. Silicon nitride bearing rollers be fabricated as nearly as possible by diamond grinding with only the roll crown added by silicon carbide grinding.

2. The postulation that grinding damage was the principal cause of poor rolling contact fatigue life of certain rods be validated by further testing of rods with what is believed to be the optimum surface preparation procedures.

APPENDIX I

Ceramics in Rolling Contact Bearings - Prior Work

Crystallized glass (Pyroceram) ceramic was examined by Zaretsky and Anderson[5] for possible use in high temperature applications. While the failure mode, a spall, was similar to that experienced with bearing steels and the scatter in life to failure was much less than that experienced with bearing steels, the so-called L_{10} of the material was less than 10 percent of that of bearing steels. Appledoorn and Royle[6] confirmed these results in a later publication. These two studies as well as others with crystallized glass including that by Carter and Zaretsky[7] indicate that if the L_{10} were at least equivalent to that of bearing steels, ceramics would be desirable because of the reduction in scatter of life to failure (associated with the absence of foreign inclusion) and because of the acceptable mode of failure. Crystallized glass perhaps was not a good candidate because of its low strength-modulus of rupture is less than 40,000 psi[8] - and low hardness - approximately 53 Rockwell C as reported in Ref. 5. In fact, if one can extract one of the more basic tenets of metal bearing practice, the crystallized glass would now not be considered because of its relatively low hardness.

Parker et al[9] conducted studies with three ceramics and one cermet for rolling contact applications with the objective being high temperature bearings. The ceramic materials were hot-pressed and cold-pressed alumina, both ninety-nine percent pure, and a two-phase sintered silicon carbide. This work was one of many that involved evaluation of aluminas, and KT silicon carbide, the latter manufactured by the Carborundum Company. Its results were representative of other work done and included five-ball tests at room temperature. Once again, life to failure for ceramics was found to have less scatter than that for bearing steels, but the L_{10} of the best material was only 7 percent of that of bearing steels. The mode of failure was a spall but attributed to a surface condition rather than subsurface stresses. Hot-pressed alumina performed the best of the three, and this better performance was related to minimum porosity, and thus better surface finish and homogeneity.

In another study, Taylor et al[10] evaluated hot-pressed silicon carbide and hot-pressed alumina for service above 1000°F, well above the operating temperature of conventional liquid lubricants. Unfortunately, rolling contact evaluations were not conducted in "standard" bearing environment.

More recently, Scott et al[11] conducted very preliminary four-ball tests with silicon nitride. While the results of these tests with the hot pressed form of silicon nitride was somewhat disappointing, the authors concluded further work with this material was in order. There is reason to believe that hot-

pressed silicon nitride the authors evaluated was substandard, as the reported hardnesses on specimens were close to a full twelve hundred points lower on the Vickers scale than that found with hot pressed silicon nitride produced by Norton Company. In addition, the authors failed to characterize the grade of hot pressed silicon nitride tested in terms of strength, density, and other important properties. The microstructure of the specimens exhibited extensive porosity.

Parker and Zaretsky[12] presented preliminary results evaluating silicon nitride at 800,000 psi Hertz stress in a NASA five ball rig. The fatigue spall in the silicon nitride resembled those in typical bearing steels. The load capacity while approximately one-third that of typical bearings steels was significantly higher than previously tested ceramic materials for rolling element bearings.

From the above mentioned studies, one can conclude that ceramics which provide better performance are those which have very low to zero porosity, have a single homogeneous phase, and exhibit a hardness at least equivalent to heat treated bearing steel.

APPENDIX II

RCF Stress Calculation

$$\sigma \text{ Max.} = \frac{C_\sigma \, C_d \, {}^3/p}{\frac{L^{2/3}}{M}}$$

Where σ max. = Max. Hertz Contact Stress, psi (not lubricated)

P = Load in Pounds

$$L = \frac{1 - \gamma_1^2}{E_1} + \frac{1 - \gamma_2^2}{E_2}$$

Where E_1, E_2 are MOE of Materials

$\gamma 1$, $\gamma 2$ are Poisson's Ratios

$$M = \frac{1}{D_1} + \frac{1}{D_2} + \frac{1}{D_1^1} + \frac{1}{D_2^1}$$

Where D's are Diameters

C_σ, C_d = Geometric Parameters

EXAMPLE:

7" Diameter steel wheels, 0.50 diameter crown
0.375" Diameter steel bar, 00 diameter crown

$E_1 = E_2 = 30 \times 10^6$ psi

$\gamma 1 = \gamma 2 = 0.29$

$$\sigma_m = \frac{C_\sigma \, C_d \, {}^3/p}{\frac{L}{M}^{2/3}}$$

$L = 6.16 \times 10^{-8}$

$M = 4.803$

$$\sigma_m = \frac{.71 \times .79 \, p^{1/3}}{5.5 \times 10^{-6}}$$

$$= 1.02 \times 10^5 \, p^{1/3}$$

$$\text{Log } \sigma \text{ max.} = \text{Log } 1.02 \times 10^5 + 1/3 \text{ Log } P$$

When P = 100 Lbs. σ max. = 475M psi

When P = 1000 Lbs. σ max. = 1,020M psi

BIBLIOGRAPHY

1. Glatz, J. W., Naval Air Propulsion Test Center, Trenton, NJ, personal communication.

2. Science of Ceramic Machining and Surface Finishing, NBS Special Publication 348, Schneider and Rice, eds., U. S. Government Printing Office, 1972.

3. Sedlacek, R. and Jorgenson, P. J., "Processing of Ceramics - Surface Finishing Studies", Final Technical Report under Contract No. N00019-70-C-0179, September 1971.

4. Pears, C. D. et.al., "A Quantitative Evaluation of test Methods for Brittle Materials", Technical Report AFML-TR-69-244, Part I, March 1970.

5. Zaretsky, E. V., and Anderson, W. J., "Rolling - Contact Fatigue Studies with Four Tool Steels and Crystallized Glass Ceramic:, J. Basic Eng. 83, 603 (1961).

6. Appledoorn, J. K., and Royle, R. C., "Lubricant Fatigue Testing with Ceramic Balls", J. ASLE 2, 45 (1965).

7. Carter, T. L., and Zaretsky, E. V., "Rolling Contact Fatigue Life of a Crystallized Glass Ceramic", NASA TN D-259 (1960).

8. Anon., "Pyroceram", Corning Glass Works, Corning, NY (undated)

9. Parker, R. J., Grisaffe, S. G. and Zaretsky, E. V., "Rolling-Contact Studies with Four Refractory Materials to 2000°F. ASLE Trans. 8, 208 (1965).

10. Taylor, K. M., Sibley, L. B. and Lawrence, J. C., "Development of a Ceramic Rolling Contact Bearing for High Temperature Use", ASME 61 Lubs-12 (1961).

11. Scott, D., Blackwell, J., and McCullagh, P. J., "Silicon Nitride as a Rolling Bearing Material - A Preliminary Assessment:, Wear 17, 73 (1971).

12. Parker, R. J., and Zaretsky, E. V., "Rolling Element Fatigue Life of Silicon Nitride Balls - Preliminary Test Results", NASA TNX-68174 (1972).